RNA-guided *As*Cas12a- and *Sp*Cas9-catalyzed knockout and homology directed repair of the *omega-1* locus of the human blood fluke, *Schistosoma mansoni*

Wannaporn Ittiprasert[1,*,#], Chawalit Chatupheeraphat[1, 2,*], Victoria H. Mann[1], Wenhui Li[1,3], André Miller[4], Taiwo Ogunbayo[4], Kenny Tran[4], Yousef Alrefaei[1,5], Margaret Mentink-Kane[4], Paul J. Brindley[1,#]

[1] Department of Microbiology, Immunology & Tropical Medicine, & Research Center for Neglected Diseases of Poverty, School of Medicine & Health Sciences, George Washington University, Washington, DC 20037, USA.

[2] Center for Research and Innovation, Faculty of Medical Technology, Mahidol University, Salaya, Nakhon Pathom, 73170 Thailand

[3] Lanzhou Veterinary Research Institute, Chinese Academy of Agricultural Sciences, Lanzhou, 730050, Gansu Province, China

[4] Schistosomiasis Resource Center, Biomedical Research Institute, Rockville, MD 20850

[5] College of Health Sciences, PAEET, Adailiya, Kuwait City, 73101, Kuwait

*, equal contribution

#, correspondence: Wannaporn Ittiprasert, wannaporni@gwu.edu, Paul J. Brindley, pbrindley@gwu.edu

Keywords: *As*Cas12a; *Sp*Cas9; ribonucleoprotein complex, CRISPR; omega-1; genome editing; homology directed repair; non-homologous end-joining; schistosome egg

Abstract

We compared the efficiency and precision of the RNA-guided *As*Cas12a nuclease of *Acidaminococcus* sp. with *Sp*Cas9 of *Streptococcus pyogenes* aiming to advance functional genomics tools for *Schistosoma mansoni*. Programmed double stranded cleavage catalyzed by *As*Cas12a results in a staggered strand break whereas *Sp*Cas9 produces a blunt ended chromosomal break. The TTTV, the optimal protospacer adjacent motif for *As*Cas12a is expected frequently within the AT-rich genome of this platyhelminth. We deployed optimized conditions (gRNA:*Sp*Cas9:DNA donor ratio and electroporation condition) to edit the *ω1* gene. *Sp*Cas9 delivered higher efficiency to mutate *ω1* target compared to *As*Cas12a for non-homology end joining (NHEJ)-catalyzed repair (14.04% *vs.* 10.88%, n = 7 replicates). Most mutations were deletions; *Sp*Cas9 induced -3 nt size deletions whereas *As*Cas12a induced deletions ranging in size from -25 to -2 nt. Although these were less absolute percentage *As*Cas12a than *Sp*Cas9 programmed mutations, the phenotypic outcomes on levels of *ω1* transcripts and expressed omega-1 protein were similar. Gene editing efficiency of *Sp*Cas9 and *As*Cas12a markedly increased in the presence of short single stranded donor templates bearing symmetrical homolog arms of 50 nt in length. With *As*Cas12a, both non-CRISPR target (NT) and target (T) strands of the *ω1* gene were tested as homology direct repair (HDR) donor templates. There were 15.67%, 28.71% and 21.43% of NHEJ from 7 pooled genomic DNA from KI_*Sp*Cas9, KI_*As*Cas12a-NT-ssODN and KI_*As*Cas12a-T-ssODN experiments, respectively. Programmed *Sp*Cas9 cleavage led to higher levels than *As*Cas12a of precise HDR mediated; 17.07%, KI_*Sp*Cas9 *vs.* 14.58%, KI_*As*Cas12a-NT-ssODN and 12.35%, KI_*As*Cas12a-T-ssODN ($P < 0.0.5$), although no significant differences in reduction in ω1 transcripts or of protein levels were apparent. These findings revealed that both *As*Cas12a and *Sp*Cas9 can provide programmed knockout and transgene insertion into genes expressed in the schistosome egg.

Introduction

Interest has increased in the use of functional genomics to investigate helminth parasites, specifically genome editing to investigate pathophysiology, carcinogenesis and biology. Recent progress has ushered in and showcased the deployment of CRISPR/Cas programmed genome editing in parasitic flatworms, in particular with the human blood fluke *Schistosoma mansoni* (Ittiprasert *et al*, 2019) and the carcinogenic liver fluke, *Opisthorchis viverrini* (Arunsan *et al*, 2019) as exemplars. However, given that these helminth parasites are non-model organisms, that the genome sequences are often not well established or curated, and that they are frequently refractory or even intractable to maintain in the laboratory or laboratory rodents, approaches to advance functional genomics investigation using the CRISPR/Cas technologies are not yet established or available for use in the field of tropical medical and neglected tropical diseases research. These fields, nonetheless, and our capacity to manage these diseases will surely be aided by advanced in gene editing technologies (Hoffmann *et al*, 2014).

RNA-guided nucleases evolved in archaea and bacteria as an for adaptive immunity mechanism to deal with and destroy phage viruses and other nucleic acid invaders (Jinek *et al*, 2012; Koonin *et al*, 2017). The catalogue of these CRISPR-Cas nucleases is expanding. The *Sp*Cas9 of *Streptococcus pyogenes,* a Class 2, Type II Cas enzyme in the phylogeny of Koonin and coworkers (Koonin *et al.*, 2017), dominates diverse gene-editing applications in biomedicine and beyond (Charpentier, 2015; Huang *et al*, 2018; Mustafa & Makhawi, 2020), given its precise double-stranded DNA (dsDNA) cleavage induced by two catalytic domains, RuvC and HNH, at sequences complementary to the guide RNA (Nishimasu *et al*, 2014). A second family of Class 2 enzymes, type V nucleases as represented by *As*Cas12a (formerly known as Cpf1), uses a single RuvC catalytic domain for guide RNA-directed dsDNA cleavage (Jeon *et al*, 2018; Zetsche *et al*, 2015). Distinct from *Sp*Cas9, *As*Cas12a orthologues recognize a T nucleotide–rich protospacer-adjacent motif (PAM), catalyze the maturation of their own guide CRISPR RNA (crRNA) and a dsDNA break distal to the PAM bearing staggered 5′- and 3′-ends (Jeon *et al.*, 2018), features that are attractive for genome editing (Malzahn *et al*, 2019). For their maturation, the crRNAs of type II CRISPR-Cas systems require processing by a cognate trans-activating CRISPR RNA (Charpentier *et al*, 2015). Moreover, the *As*Cas12a endonuclease is smaller than *Sp*Cas9 in size and uses a shorter CRISPR RNA (crRNA) for activity (Liu *et al*, 2017). Notably, target site activated *As*Cas12a exhibits non-specific *trans* activity against bystander nucleic acids (Chen *et al*, 2018; Smith *et al*, 2020), an attribute that has enabled its application in a burgeoning range of biosensors (Kellner *et al*, 2019; Li *et al*, 2018a).

Delivery of CRISPR reagents into the cells of the multicellular parasite *S. mansoni* in the form of ribonucleoprotein (RNP) complexes can enable immediate and permanent programmed gene editing and obviate concerns with CRISPR reagent longevity or integration in the host cell genome. Programmed CRISPR-editing using RNP-based delivery can precede analysis of mutated target regions that rely on cloning and vector construction steps. Previously, we deployed both RNPs and lentiviral-delivered CRISPR/*Sp*Cas9 approaches to knock-out (KO) and knock-in (KI) into a blunt end at *Sp*Cas9 cleavage site at the multiple copies of the omega-1 (*ω1*) gene in parasite eggs. To advance functional genomics for schistosomes and aiming to improve the mutagenesis and transgene knock-in of CRISPR efficiency in schistosomes, which exhibit AT-rich genomes, we investigated the nuclease activity of Cas12a of *Acidaminococcus* sp. (*As*Cas12a) in contrast with Cas9 of *S. pyogenes* (*Sp*Cas9). These CRISPR systems differ in two

90 main aspects: 1) *Sp*Cas9 recognizes NGG as the protospacer adjacent motif (PAM) whereas
91 *As*Cas12a recognizes the T-rich, TTTV; 2) Catalysis by *Sp*Cas9 results in blunt double stranded
92 DNA at three nucleotides 5' to the PAM whereas *As*Cas12a results in a staggered cleavage at 23
93 nt (target strand; T) and 18 nt (non-target strand; NT) 3' to the PAM (Banakar *et al*, 2020).
94 Comparisons of these two RNA-programmed nucleases in the context of the *ω1* gene of *S.*
95 *mansoni* may inform decisions for functional genomics manipulations aiming to enhance
96 efficiency of homology directed repair (HDR) targeting genes expressed by the developing
97 schistosome egg and other developmental stages (Ittiprasert *et al.*, 2019; Sankaranarayanan *et al*,
98 2021; Takaki *et al*, 2021a; Takaki *et al*, 2021b).

99 **Results**

100 **The *omega-1* multicopy gene, guide RNAs, and single stranded DNA donor templates**

101 The gene editing efficiency of *Sp*Cas9 and *As*Cas12a was compared in assays targeting the
102 *omega-1* gene which encoded a T2 ribonuclease that is secreted by the mature egg of *S. mansoni*
103 into the surrounding host tissues and circumoval granuloma (Schwartz & Fallon, 2018).
104 Specifically, the four copies of *omega-1*, well annotated in WormBase Parasite (Bolt *et al*, 2018)
105 (update of 16 September 2021) as hepatotoxic ribonuclease – Smp_334170.1, Smp_334170.2,
106 Smp_334240, and Smp_333930, were targeted for design of gRNAs and donor repair templates.
107 These four copies reside on chromosome 1 of *S. mansoni*, with reverse strand positions at
108 3,980,364 to 3,984675, 3,992,964 to 3,995,246 and 3,908,953 to 3,911,250 (PRJEA36577),
109 respectively. These copies share >99% nucleotide sequence identity, are ~2.3 kb in length, are
110 highly AT rich (65%), and encode an enzyme of 127 (Smp_334170.2, Smp_334240 and
111 Smp_333930) or 115 (Smp_334170.1) amino acid residues in length. Smp_333220, also located
112 on chromosome 1 at 3,925,420-3,927,716 but lacking annotation on the *S. mansoni* annotated
113 genome version 7_2021, was also included. Smp_333220 shares >99% chromosomal and
114 mRNA sequence identity with the three *ω1* copies (Fig S1B). Guide RNAs for *Sp*Cas9 and
115 *As*Cas12a designed with the assistance of CHOPCHOP both target the same region of exon 1 of
116 *omega-1*, disrupting its catalytic active site histidine (Luhtala & Parker, 2010), with the
117 programmed cleavage sites for Cas in close proximity, separated by three nucleotides (Fig 1A
118 and B).

119 We designed three single stand oligodeoxynucleotide (ssODN) donors for homology directed
120 repair (HDR) of *ω1* following programmed mutation. Given the differing PAM requirements of
121 *Sp*Cas9 and *As*Cas12a as well as the divergent formats of the DSB, blunted ended by *Sp*Cas9 and
122 sticky ended by *As*Cas12a, the designs differed for the ssODNs for use with each nuclease.
123 Based on earlier findings (Ittiprasert *et al.*, 2019), the design of the ssODN donors included 3'
124 and 5' homology arms (HA) of each of 50 nt in length, complementary to the target strand for
125 *Sp*Cas9 and for *As*Cas12a, for either the target strand, termed *Sp*Cas9-T-ssODN, or for the non-
126 target strand donor, termed *As*Cas12a-NT-ssODN. Note that sequences identical to the PAM for
127 *As*Cas12a and ~18 nt of the protospacer region were retained within the 5'-HA of *As*Cas12a-T-
128 ssODN (Fig 1B and C).

129

130 **Absence of *trans* activity of activated *As*Cas12a against the ssODN donors**

131 Previous reports dealing with *Lachnospiraceae bacterium* ND2006 and *Francisella novicida*
132 *As*Cas12a describe indiscriminate *trans*-activity unleashed on ssDNA after gRNA activation and
133 target binding of *As*Cas12a (Chen *et al.*, 2018; Gier *et al*, 2020). Given that our goal here was to
134 compare *Sp*Cas9 and *As*Cas12a in schistosomes, and given that we used an orthologous
135 *As*Cas12a from *Acidaminococcus* sp. BV3L6 (IDT), in both KO and KI assays, we sought to
136 confirm whether the *omega-1* target gene activated *As*Cas12a might exhibit also *trans*-activity
137 against the donor single stranded templates that we planned to use in KI assays, *As*Cas12a-T-
138 ssODN and *As*Cas12a-NT-ssODN, in addition to RNA-guided double stranded DNA cleavage
139 activity.

140 Accordingly, we also carried out *in vitro As*Cas12a nuclease activity assays using RNPs targeting
141 a 426 bp amplicon of the exon 1 of *omega-1* (

142 A, 2B and 2C). These assays confirmed that the crRNA was highly active and following
143 incubation at 37°C for 30 min had cleaved the double stranded amplicon at the programmed
144 cleavage site into two fragments of 265 and 161 bp, as expected (Fig 2B; Agilent Bioanalyzer
145 electropherogram). In contrast, the activated *As*Cas12a-RNP complex failed to digest either of
146 the single stranded templates, ssODNs *As*Cas12a-T-ssODN or *As*Cas12a-NT-ssODN after 120
147 min at 37°C (Fig 2C). As seen in the electropherogram, the ssODNs remained intact at 124 nt.
148 Single stranded DNA standards ranging in size from 200 to < 40 nt were included in the assay
149 (Fig 2C). In summary, the findings suggested that *omega-1* target gene activated As*As*Cas12a
150 would not exhibit indiscriminate *trans*-nuclease activity against the ssODNs within schistosome
151 cells, although an *in vitro* surrogate assay cannot faithfully mimic conditions within a viable
152 schistosome egg.

153 **Estimation of CRISPR efficiency of *Sp*Cas9 and *As*Cas12a**

154 RNP complexes of *Sp*Cas9-sgRNA and *As*Cas12a-CRISPR RNA (crRNA) targeting *ω1* were
155 delivered to the LE by electroporation (Ittiprasert *et al.*, 2019). The efficiency of programmed
156 mutation was assessed by TIDE analysis of Sanger sequence chromatograms (Gier *et al.*, 2020;
157 Jacobsen *et al*, 2020), followed by targeted amplicon NGS and analysis of the reads using
158 CRISPResso2 (Pinello *et al*, 2016). Twelve independent biological replicates were carried out.
159 *As*Cas12a programmed KO led to significantly more indels than were induced with *Sp*Cas9 *(P* <
160 0.001, paired, two-tailed $t = 7.450$, df = 11) (Fig 2G and H). The mean CRISPR efficiency for
161 KO with *Sp*Cas9 was 0.89%±0.43 (range, 0.30-1.31%) and 1.83%±0.29 (range, 1.39-2.54%)
162 with *As*Cas12a, when compared with the control (mock) groups. KI efficiency also was
163 investigated for individual replicates by TIDE and for pooled samples by analysis amplicon NGS
164 (Illumina) reads. Programmed mutation by *Sp*Cas9 was more efficient in the presence or absence
165 of donor ssODN, i.e., KI *versus* KO groups, 1.43±0.4, range 0.51-2.31% (Fig 2G and H). By
166 contrast, differences in mutation efficiency were not apparent between the KO and KI groups
167 using *As*Cas12a; 1.75%±0.63 (range 1.11-2.69%) and 1.54%±0.49 (range 1.82-2.20%) for
168 *As*Cas12a-NT ssODN and *As*Cas12a-T ssODN, respectively.

169 **Quantification of transgene copy number by external standard curve**

170 The external standard curve design that we employed to estimate transgene copy number in
171 genomics DNA of the schistosome eggs estimates transgene copy number by comparison with an
172 external standard curve (Fig 2E and F). The standard curve on simple linear regression (y = -
173 4.0964ln[10] + 44.821, R^2 = 0.9923) was established with logarithm-10 transformed initial DNA
174 input, plasmid pCR4, which encodes the six stop codon cassette (Ittiprasert *et al.*, 2019), as the
175 dependent and the Ct value from the qPCRs as the independent variable (not shown). We
176 estimated the transgene copy number on the 5' and 3' of KI site in *ω1* by converting the
177 measured Ct values to log copy numbers using the equations obtained from the standard curves.
178 Subsequently, dividing the means by the antilog of each result, we arrived at an estimate of the
179 transgene copy number. A 790 bp product amplified for the control wildtype sequence and
180 amplicons of 235 bp and 182 bp for the 5' and 3' flanking regions, respectively, of the KI
181 genomic DNA containing the six stop codon transgene were analyzed, which revealed 3'-side
182 transgene integration values of 3.61±0.25, 4.44±0.84 and 4.19±1.22 from the KI_*Sp*Cas9,
183 KI_*As*Cas12a-NT-ssODN and KI_*As*Cas12a-T-ssODN treatment groups, respectively (*P* =
184 0.4057, = 0.6264 and = 0.9155; NS; one-way ANOVA, multiple comparisons, 95% CI for
185 differences of the means) (Fig 2E). However, the presence of asymmetrical HDR was revealed
186 by significant differences among the copy number values for the 5' side transgene integration
187 estimates: 2.72±0.42, 5.06±0.54, and 1.64±0.39 for the KI_*Sp*Cas9, KI_*As*Cas12a-NT-ssODN
188 and KI_*As*Cas12a-T-ssODN groups, respectively (Fig 2F; *P* = 0.0214, *P*=0.0001 and *P* < 0.0001,
189 *,***, ****, respectively; one-way ANOVA, multiple comparisons).

190 **Estimates of indels from NHEJ and/or HDR using NGS reads from targeted amplicons**

191 Pooled gDNAs (above) also were used as templates for targeted amplicons for NGS and
192 CRISPResso2 employed to assess the efficiency of transgene KI from HDR in the NGS reads.
193 Comparison of the mutations among all four copies of the *ω1* gene also were undertaken. From
194 Whereas TIDE analysis using Sanger direct sequencing chromatograms was used above to
195 estimate % efficiency of CRISPR manipulations in individual biological replicates, here targeted
196 amplicons from pools of gDNAs from the biological replicates was used to acquire libraries of
197 reads (Amplicon EZ, Genewiz). More than 150,000 reads from each NGS library were obtained.
198 Analysis of the reads using CRISPResso2 provided increased sensitivity of detection of
199 programmed gene editing than TIDE, as expected (Sentmanat *et al*, 2018). Specifically, there
200 were 12.26%, 1.66%, 0.12% modified sequence (NHEJ) for KO-*Sp*Cas9 and 9.27%, 1.33% and
201 0.28% of NHEJ for KO-*As*Cas12a, when compared with the WormBase Parasite reference
202 sequence (identical amplicon from Smp_334170.1, Smp_334170.2, Smp_334240), Smp_333930
203 and Smp_333870, respectively (Fig 3A and B). A small number of reads were assessed to be
204 ambiguous by CRISPResso2, 0.49% and 0.93% for KO-*Sp*Cas9 and KO-*As*Cas12a, respectively
205 (Fig 3A and B). Deletions were the only type of indel detected, for both *Sp*Cas9 and *As*Cas12a.
206 In like fashion to other studies (An *et al*, 2020; Dumeau *et al*, 2019; Kissling *et al*, 2019),
207 deletion of large sizes resulted from programmed *As*Cas12a editing (from -2 bp to -26 bp
208 deletion size) a the programmed DSB, compared to -3 bp at the DSB programmed from *Sp*Cas9
209 (Fig 3C and D provide representative allele sequences). Both enzymes showed a preference to
210 mutate the reference Smp_334170 copy, and also Smp_334240, rather than the Smp_333930
211 and/or Smp_333870 copies of *omega-1*. The numbers of indels arising from NHEJ with *Sp*Cas9
212 and with *As*Cas12a both increased in the presence of a ssODN donor repair template. The total
213 NHEJ were 15.67%, 28.71% and 21.43% from KI-*Sp*Cas9-NT-ssODN, KI-*As*Cas12a-NT-
214 ssODN and KI-*As*Cas12a-T-ssODN, respectively (Fig 4A, B and C). Deletion size as

215 determined by CRISPResso2 for the KI-*Sp*Cas9 group was larger than for KO-*Sp*Cas9,
216 increasing up to -13 bp length deletions. Similarly, base deletion size from KI-*As*Cas12a was
217 larger than KO-*As*Cas12a with deletion of -42 bp detected (Fig 4D, E and F). Levels of
218 ambiguous results were estimated at 1.66%, 1.03% and 0.73% from KI-*Sp*Cas9, KI-*As*Cas12a-
219 NT-ssODN and KI-*As*Cas12a-T-ssODN, respectively.

220 To estimate the HDR events, we included the donor sequence as a parameter in the
221 CRISPResso2 analysis. More HDR events mediated by CRISPR/*Sp*Cas9 were detected than with
222 CRISPR/*As*Cas12a; 17.07% *vs* 14.56% and 12.37%, in like fashion to our earlier findings
223 (Santos *et al*, 2021). However, in *Sp*Cas9 sample, more imperfect HDR was seen (0.94%) than
224 in the *As*Cas12a groups (0.41% and 0.68%) (Fig 4A, B, C, G, H and F). Frequently, imperfect
225 HDR event alleles from both Cas nucleases were missing several residues (2-5 nt) on the 5' side
226 of the programmed DSB. We note that this mutation repair outcome may have impacted
227 quantification of the 5' KI transgene copy number, especially in KI-*As*Cas12a-T-ssODN samples
228 which contained 5 nt imperfect HDR repair on the six stop codon cassette (primer probing
229 sequence). Imperfect HDR at the 5' side might result from synthesis-dependent strand annealing
230 (Straume *et al*, 2020).

231 **Transcription of *ω1* interrupted by programmed mutation by *Sp*Cas9 and *As*Cas12a**

232 Primers specific for the four annotated copies of *ω1* were employed to investigate transcription
233 by real time quantitative PCR (Fig S1C). Relative expression levels of *ω1* mRNA in negative
234 controls and experimental KO or KI eggs were compared with wild type. Significantly reduced
235 levels of *ω1* were seen in eggs following the experimental the CRISPR manipulations for gene
236 KO and KI. Transcription of *ω1* was reduced, as follows: 63.76%±5.57, 76.88%±11.33,
237 71.81%±10.91, 98.69%±0.44 and 80.04%±0.09 in the KO_*Sp*Cas9, KI_*Sp*Cas9, KO_*As*Cas12a,
238 KI_*As*Cas12a-NT-ssODN and *As*Cas12a-T-ssODN groups, respectively. Notably, LE subjected
239 to KI_*As*Cas12a_NT-ssODN retained <2% ω1 transcript levels of the mock control (Fig 5A),
240 and the level in the KI_*As*Cas12a-NT-ssODN group was significantly lower than the
241 KI_*As*Cas12a-T-ssODN group, KI_*Sp*Cas9-ssODN. Significant differences were not apparent
242 between the KO_*Sp*Cas9 and KO_*As*Cas12a groups, generally. There were minor differences in
243 levels of transcription among the negative control groups (Fig 5A). Differences among treatment
244 groups were assessed using ANOVA with multiple comparisons (P values < 0.01 to < 0.0001; n=
245 4; F = 11.77).

246 **Protein levels ascertained by western blotting**

247 An anti-rω1 rabbit IgG was used to investigate levels of omega-1 in lysates (SEA) of LE. SEA
248 (200 ng) from the three controls, i.e., the mock, enzyme only, and mixed sgRNAs only groups,
249 and from the KO and KI groups with *Sp*Cas9 or *As*Cas12a was size fractionated by SDS-PAGE
250 and transferred to PVDF and probed with the rabbit antibody (Fig 5B). Following densitometric
251 analysis of the resulting signals, the levels of omega-1 remaining in the SEA were estimated at
252 64%±11.65, 43.88%±6.02, 49.27%±4.19, 37.9%±2.28 and 52.16%±10 in the KO_*Sp*Cas9,
253 KI_*Sp*Cas9, KO_*As*Cas12a, KI_*As*Cas12a-NT-ssODN and KI_*As*Cas12a-T-ssODN groups,
254 respectively. The differential intensity of ω1expression was not diminished among the sgRNA
255 only groups (Fig 5B and C). By contrast, ω1 protein levels were markedly diminished among all
256 the experimental treatment groups when compared with the controls (P <0.0001) (ANOVA, F =

257 27.05 , n = 4). Significant differences among for levels of ω1 among the KO and KI SEA
258 samples were not apparent (Fig 5C).

259 **Discussion**

260 Given the central role of the egg and its secretions in disease and in the transmission of
261 schistosomiasis (Costain *et al*, 2018), and given the potential of CRISPR/Cas gene editing to
262 advance understanding of this and other neglected tropical disease pathogens, we posit that
263 access to omega-1-negative eggs will provide an informative tool to confirm the role of this
264 ribonuclease in disease transmission. Functional knockout (KO) of the *omega-1* gene and the
265 resulting immunologically impaired phenotype have showcased the novel application of
266 CRISPR/*Sp*Cas9 and its utility for functional genomics in schistosomes (Hsu *et al*, 2014; Jinek *et*
267 *al.*, 2012). In view of this progress, and the demonstrated tractability of *Sp*Cas9-catalyzed KO of
268 the *omega-1* gene, here compared the performance of a second RNA-guided Cas nuclease, in
269 terms of efficiency and precision, with *Sp*Cas9 and the *As*Cas12a nuclease of *Streptococcus*
270 *pyogenes* and *Acidaminococcus* sp. We now report that the efficiency of RNA guided
271 programmed knock-out of ω1 by *As*Cas12a was superior to *Sp*Cas9.

272 In this investigation, the RNA-guided target region for programmed mutation included PAMs for
273 both *Sp*Cas9 and *As*Cas12a within three nucleotides of each other within exon 1 of the coding
274 region of the omega-1 gene. The optimal protospacer adjacent motif for *As*Cas12a, TTTV
275 (Swarts & Jinek, 2019; Zetsche *et al.*, 2015), is expected to occur abundantly in the AT rich
276 genome of *S. mansoni* (Protasio *et al*, 2012; Zetsche *et al.*, 2015). Programmed double stranded
277 cleavage catalyzed by *As*Cas12a results in a staggered strand break of the target gene sequence
278 that may enhance efficiency of homology directed repair (HDR) (Swarts & Jinek, 2019). When
279 RNPs assembled from the nuclease and cognate crRNA, *As*Cas12a was significantly more
280 efficient than *Sp*Cas9 for KO, presumably reflected non-homology end joining (NHEJ)-catalyzed
281 repair and gene silencing. Specifically, the KO efficacy of *As*Cas12a was significantly higher
282 than that to *Sp*Cas9; 1.8% versus 0.9%, respectively. Greater mutation efficacy for versions of
283 *As*Cas12a over *Sp*Cas9 have been reported but, on the other hand, the reverse outcome has been
284 described (Hur *et al*, 2016; Kim *et al*, 2016). Comparisons among studies are not
285 straightforward because of differences in species, target genes, delivery method, and
286 temperature, among other confounders. In addition, there are three widely used orthologues of
287 *As*Cas12a, *Fn*Cas12a from *Francisella novicida U112*, *Lb*Cas12a from *Lachnospiraceae*
288 *bacterium ND2006*, and *As*Cas12a from *Acidaminococcus* sp. *BV3L6* and these have been tested
289 in diverse target eukaryotic species (Mustafa & Makhawi, 2020). (Other orthologues have also
290 been studied (Tóth *et al*, 2018; Zhang *et al*, 2021).) *As*Cas12a in active at 37°C whereas other
291 orthologues are catalytically active at lower temperatures, which has enabled their deployment in
292 research targeting zebrafish (Liu *et al*, 2019), insects, and maize (Zhang *et al.*, 2021), and
293 environmental and diagnostic biosensing (Chen *et al.*, 2018; Ma *et al*, 2020; Nguyen *et al*, 2021).

294 We compared these two CRISPR methods for programmed gene editing of the well-known
295 omega-1 extracellular T2 ribonuclease secreted by the mature egg of *S. mansoni*, which is a key
296 modulator of pathogenesis and transmission (Costain *et al.*, 2018; Everts *et al*, 2009; Schwartz &
297 Fallon, 2018; Steinfelder *et al*, 2009). We investigated HDR-mediated gene editing with HiFi-
298 *Sp*Cas9 or *As*Cas12a delivered by electroporation in the presence of the RNPs and donor repair
299 templates donors. We designed the guide RNAs to anneal to protospacer regions that we

300 essentially at the same site of the gene. The programmed DSB were separated by only three
301 nucleotide residues, on the non-target strand of the target gene. Each donor ssODN template for
302 *Sp*Cas9- and *As*Cas12a-programmed KI included a transgene cassette of 24 nt in length with six
303 stop codons (Ittiprasert *et al.*, 2019) but in which the homology arms differed slightly on the non-
304 target strand due to the position of the predicted DSB. For programmed KI with
305 CRISPR/*As*Cas12a, we also included as the transgene, the reverse complement sequence of the
306 six stop codon cassette flanked by the target stand sequence as the homology arms, given
307 concern with respect to indiscriminate trans-activity by activated *As*Cas12a against random
308 single stranded DNA, and especially for the ssODN with NT homology arms which retains the
309 PAM and partial (~18 nt) protospacer sequence (Swarts, 2019; Swarts & Jinek, 2018, 2019).
310 RNA-guided *Sp*Cas9 cleavage led to higher level (~4% higher) of precise KO compared to that
311 obtained with *As*Cas12a but markedly less, ~6-13%, precise KI. Deletions were the frequent
312 mutation type seen with both *Sp*Cas9 (deletions of -3 nt in length) and *As*Cas12a (deletions of -
313 26 nt to -2 nt in length) due to NHEJ repair. Using conditions optimizing previously for *Sp*Cas9
314 KI (Ittiprasert *et al.*, 2019), here CRISPR/*Sp*Cas9 induced higher (~3%) HDR levels than
315 CRISPR/*As*Cas12a to insert the transgene into the *ω1* target for both *As*Cas12a-NT-ssODN and
316 *As*Cas12a-T-ssODN donors. Characterization of both *Sp*Cas9-and *As*Cas12a-edited eggs
317 revealed reductions in levels of both of *ω1* mRNAs and of expressed ω1 protein. Together, these
318 outcomes indicated that both of the CRISPR/Cas systems mutated this key schistosome egg
319 gene. Further optimization of the *As*Cas12a-based approach with regard to gRNA:*As*Cas12a
320 and/or gRNA:*As*Cas12a:ssODN ratios, format of donor(s), and/or temperature manipulation
321 likely will be informative.

322 A spectrum of chromosomal alleles was apparent following programmed KI of single stranded
323 DNA (ssDNA) repair templates of 124 nt in length with 5'- and 3'-homology arms specific for
324 the predicted cleavage sites of each nuclease. Both target strand (T) and non-target strand (NT)
325 ssDNA donors were tested. Accurate HDR was catalyzed by both *Sp*Cas9 and *As*Cas12a, and
326 these accounted for a minority of the payload integration events. The two sides of the
327 programmed *As*Cas12a double-strand break were repaired by apparently separate pathways since
328 mutant alleles that included only the left or only the right side of the donor transgene were
329 frequent although accurate HDR was significantly more likely in the presence of the NT
330 compared with T donor. Overall, *As*Cas12a was more efficient than *Sp*Cas9 for RNA-guided
331 knockout whereas both *Sp*Cas9 and *As*Cas12a catalyzed similar levels of accurate transgene
332 insertion at this model *ω1* gene target. These findings may be expected based on reports with
333 other cells and species that indicate that integration of repair template is not always precise (Paix
334 *et al*, 2017; Ranawakage *et al*, 2020) and *Sp*Cas9 shown even higher levels of HDR correction
335 than *As*Cas12a (Santos *et al.*, 2021), including in HEK293T and pluripotent stem cells where
336 mis-integrations patterns indicate that two sides of a DSB are repaired by separate cellular repair
337 pathways including the involvement of microhomology as a driver of the mis-integration.

338 In addition to its guide RNA programmed gene editing and double stranded DNA cleavage
339 activity, *As*Cas12a and related Type 2 subtypes V and VI nucleases display target substrate
340 bound non-specific trans-activity against ssDNA, dsDNA and/or RNA (Fuchs *et al*, 2019;
341 Nguyen *et al*, 2020). Accordingly, we speculated that activated *As*Cas12a associated with the
342 target exon 1 site in omega-1 may digest the donor ssODN provided as the repair template. If so,
343 investigation of comparative efficiency of *As*Cas12a *versus Sp*Cas9 catalyzed knock-in would
344 have been compromised. To investigate this possibility, we performed a series of in vitro assays

345 using non-activated and activated *As*Cas12a. Under the conditions and time frame of the
346 reactions (commercial *As*Cas12a, 37°C, 100 mM NaCl, 120 min reaction duration), we failed to
347 detect any marked degradation of the ssODN. Although this assay did not reflect the condition *in*
348 *vivo* in the transfected schistosome eggs, lack of apparent *As*Cas12a trans-activity *in vitro* may
349 not accurately reflect the situation within the nucleus of the cells within the egg: the RNP may
350 not have been retained at the programmed target site - degraded by cellular enzymes and/or
351 displaced by the cellular repair machinery-following cleavage before trans activity damaged the
352 donor ssODN and/pr other phenomena including protection of cellular DNA by histones.
353 Nonetheless, both *Sp*Cas9 and *As*Cas12a delivered similar knock-in performance in the eggs.

354 *As*Cas12a provided enhanced programmed knockout activity compared to *Sp*Cas9 at a specific
355 target site in the *omega-1* gene locus but both exhibited similar performance for HDR based
356 transgene insertion. Whereas these findings do not enable extrapolation to similarly superior
357 performance of *As*Cas12a for CRSISR/Cas-based gene editing of other schistosome genes and
358 for insertion of transgenes, and yet given the central role of the schistosome egg in
359 schistosomiasis, the approach demonstrated here does expand the toolkit for functional genomics
360 in helminth parasites (Sankaranarayanan *et al.*, 2021; Zamanian & Andersen, 2016). *As*Cas12a
361 will find use or gene editing AT rich genomes, such as in schistosomes and other parasitic
362 platyhelminths (International Helminth Genomes, 2019) although optimizing editing protocols
363 including time, temperature, metal ion concentration of editing reactions, donor format, donor
364 length, and guide RNA modifications, and other parameters will influence performance (Chen *et*
365 *al.*, 2018; Hendel *et al*, 2015; Swarts & Jinek, 2018). Lastly, since transgene insertion into the
366 zygote within the newly released egg has already been described and shown to enable
367 establishment of lines of transgenic schistosomes, advances with gene editing approaches to this
368 key developmental stage of the schistosome life cycle portend progress in the near future with
369 informative gain-of-function lines of transgenic schistosomes.

370

371 **Materials and Methods**

Reagent/Resource	Reference or Source	Identifier or Catalog Number
Experimental Models		
Schistosoma mansoni eggs	Schistosomiasis Resource Center, Biomedical Research Institute, Maryland, USA	
Swiss Inbred mice (*M. musculus*)	The Jackson Laboratory	SWR/J
Recombinant DNA		
rocombinant omega-1 protein	Dr. Ron Hokke	Gifted from Dr. Ron Hokke
Antibodies		
Polyclonal antibody against recombinant omega-1 protein	Research Resource Identifier (RRID)	AB_2889886
goat anti-rabbit IgG (H+L) horse radish peroxidase conjugate	Life Technologies, Thermofisher Sciences	Cat # 31460
Oligonucleotides and sequence-based reagents		
PCR primers	This study	Synthesized from IDT
ssODN	Ittiprasert *et al*., 2019 and this study	Ultramer DNA Oligos, Synthesized from IDT
synthetic guide RNA	Ittiprasert *et al*., 2019 and this study	Synthesized from IDT
Chemicals, enzymes and other reagents		
Alt-R® CRISPR-Sp HiFi Cas9 enzyme V3	Integrated DNA Technologies	1081060
Alt-R® CRISPR-AsCas12a enzyme V3	Integrated DNA Technologies	1081068
DNAzol® ES reagent	Molecular Research Center	DN127
RNAzol® RT Reagent	Molecular Research Center	RN190
Opti-MEM	FisherScientific	Gibco™ 31985062
DMEM	FisherScientific	88364
fetal bovine serum	FisherScientific	Gibco™ 26140079
100x Penicillin-Streptomycin-Fungizone	FisherScientific	SV30079.01
NucleoSpin® Gel and PCR clean up	Takara	740609

SsoAcvanced Universal SYBR Green Supermix	BioRad	1725271
RIPA buffer	Millipore-Sigma	R0278-500ML
Bradford reagent	BioRad	5000201
SDS-PAGE polyacrylamide gradient gels, 4-12% gel, w/v	ThermoFisher Scientific	NP0322PK2
Maxima First Strand cDNA Synthesis Kit for RT-qPCR, with dsDNase	ThermoFisher Scientific	K1672
Peroxidate substate; Clarity™ Western ECL Substrate	BioRad	1705062S
GoTaq® Green Master Mix	Promega	M712
NEB buffer 2.1	NEB	B720S
Proteinase K	ThermoFisher Scientific	EO0491
Agilent DNA 1000 Kit	Agilent Technologies	5067-1505
Agilent small RNA kit	Agilent Technologies	5067-1548
Software		
CHOPCHOP	http://chopchop.cbu.uib.no/	
TIDE	https://tide.deskgen.com/	
CRISPREsso2	https://crispresso.pinellolab.partners.org/submission	
SnapGene	https://www.snapgene.com/	Academic Subscription Plan
GraphPad Prism	Prism software	Monthly Subscription Plan
Other		
CFX96 Touch Real-Time PCR Detection System	BioRad	
ElectroSquarePorator	BTX	ECM830
Chemi-Doc MP System	BioRad	
BioAnalyzer	Agilent Technology	

374 **Ethics statement**

375 Mice experimentally infected with *S. mansoni*, obtained from Schistosomiasis Resource Center
376 (SRC) at the Biomedical Research Institute (BRI), MD were housed at the Animal Research
377 Facility of the George Washington University (GWU), which is accredited by the American
378 Association for Accreditation of Laboratory Animal Care (AAALAC no. 000347) and has an
379 Animal Welfare Assurance on file with the National Institutes of Health, Office of Laboratory
380 Animal Welfare, OLAW assurance number A3205-01. All procedures employed were consistent
381 with the Guide for the Care and Use of Laboratory Animals. The Institutional Animal Care and
382 Use Committee (IACUC) at GWU approved the protocol used for maintenance of mice and
383 recovery of schistosomes. Swiss albino mice were euthanized seven weeks after infection with *S.*
384 *mansoni*, livers were removed at necropsy, and schistosome eggs recovered from the livers
385 (Dalton *et al*, 1997). The 'liver eggs, termed LE' population is expected to include eggs of a
386 spectrum of age ranging from newly released by the female schistosome through to mature eggs
387 containing a fully developed miracidium (Jurberg *et al*, 2009). LE were maintained in DMEM
388 medium supplemented with 10% heat-inactivated fetal bovine serum (FBS), 2%
389 streptomycin/penicillin at 37°C under 5% CO_2 in air for 18-24 hours before use in gene editing
390 assays (below) (Dalton *et al.*, 1997; Ittiprasert *et al.*, 2019; Lu *et al*, 2021; Mann *et al*, 2010;
391 Mann *et al*, 2014).

392 **CRISPR/Cas target design and single stranded DNA donors**

393 The *ω1*-gene specific gRNA for *Sp*Cas9 and *As*Cas12a were designed to target all four copies of
394 the hepatotoxic ribonuclease *omega-1* gene. All four are located on *S. mansoni* genome update
395 annotation of version 7 (updated 16-September-2021 on WormBase ParaSite,
396 https://parasite.wormbase.org/Multi/Search/Results?species=all;idx=;q=Hepatotoxic%20ribonucl
397 ease%20omega-1;site=ensemblunit&filter_species=*Schistosoma_mansoni*_prjea36577);
398 Smp_334170.1, Smp_334170.2, Smp_334240 and Smp_333930 by an online CRISPR design
399 tool, CHOCHOP (Labun *et al*, 2016; Labun *et al*, 2019; Montague *et al*, 2014). There are 99-
400 100% sequence and coding sequence identity among those copies (Fig S1A), which encoding an
401 enzyme of 115amino acids in length, respectively. These *ω1* copies are located on chromosome
402 1 at nucleotide (nt) position 3980364 to 3984675, 3992964 to 3995246, and 3908953 to
403 3911250, respectively. The guide RNA (gRNA), which targets exon 1 of *ω1* complimentary to
404 the catalytic active site histidine [within FRKHEFEKHGLCAVEDPQV] codons, for the gRNAs
405 programming both *Sp*Cas9 and *As*Cas12a. In addition, the gRNAs exhibited similarly high
406 predicted CRISPR efficiency scores along with an absence of predicted off-target cleavages, as
407 predicted using the CHOPCHOP algorithm using Smp_334170.2 as template (Fig 1A and B).
408 Specifically, the sequence of the gRNA used with *Sp*Cas9 was 5'-
409 GCATGGTTTGTGTGCAGTTG-3', 20 nt in length and that for *As*Cas12a was 5'-
410 AAAAGCATGGTTTGTGTGCA -3', 20 nt on exon 1 of Smp_334170.2, Smp_334240 and
411 Smp_333930 or exon 4 of Smp_334170.1 (Fig S1A) The expected cut sites of two nucleases are
412 discrete, being 3 and 2 nt apart from each other on the non-target (NT) and target (T) strands,
413 respectively (Fig 1A).

414 Single stranded oligonucleotide donors (ssODN) were designed to insert the 24 bp encoding six-
415 stop codons into the programmed cleavage target. The homology arms used in the ssODN donor
416 with *Sp*Cas9 was the non-target strand flanking both the 3' and 5' sides of the blunt ended DSB,

417 termed here *Sp*Cas9-ssODN. The homology arms of the two donor ssODNs used with *As*Cas12a
418 (cut at 18 nt and 23 nt on NT and T strands, leading to a sticky ended DSB) were either the target
419 stand or the non-target strand sequences (Fig 1B and C), here termed *As*Cas12a-NT-ssODN and
420 *As*Cas12a-T-ssODN, respectively. The complementary reverse of the 24 nt stop codon cassette
421 was used in the *As*Cas12a-T-ssODN donor, aiming for HDR insertion of the stop codons in the
422 translated forward strand of the gene (Fig 1C).

423 **CRISPR reagents**

424 Alt-R® CRISPR-*Sp*Cas9 and Alt-R® CRISPR-*As*Cas12a reagents (Alt-R® S.p. HiFi Cas9
425 nuclease V3, synthetic gRNA (sgRNA) (Labun *et al.*; Labun *et al.*; Nishimasu *et al.*), Alt-R® As
426 *As*Cas12a V3 and crRNA), and ssODN HDR donor templates (Ultramer DNA oligos) and Alt-
427 R® *Sp*Cas9 or *As*Cas12a Electroporation enhancer buffers were from Integrated DNA
428 Technologies (IDT) (Coralville, IA). Figure 1C provides the nucleotide sequences of the gRNAs
429 and donor ssODNs.

430 **Ribonucleoprotein (RNP) assembly and delivery by electroporation**

431 Stock solutions of the gRNAs for use with *Sp*Cas9 and *As*Cas12a and of the ssODNs were
432 prepared at 1.0 µg/µl in Opti-MEM medium (Sigma, St. Louis, MO). Each gRNA was
433 combined with the respective nuclease at 1:1 ratio to form an RNP complex (Ittiprasert *et al.*,
434 2019). The mixture was incubated at 23°C for 15 min, after which 3 µl of Alt-R® *Sp*Cas9 or
435 *As*Cas12a electroporation enhancer was added. The mixture was transferred to a chilled 4 mm
436 electroporation cuvette (BTX), containing ~ 5,000 LE in 100 µl Opti-MEM. LE in the presence
437 of RNPs and the other reagents were subjected to square wave electroporation with a single 125
438 volts, 1 pulse for 20 ms (ElectroSquarePorator, ECM830, BTX San Diego, CA). In KI assays, 6
439 µg of ssODN was included in the cuvette before electroporation. Following delivery of the
440 RNPs, LE were maintained for 10 days at 37°C, 5% CO_2 in air. In addition to experimental gene-
441 edited groups, control groups included LE electroporated in Opti-MEM (mock), mixed-Cas
442 enzymes only, mixed-sgRNAs only, and mixed-ssODNs only. Experimental and control groups
443 were otherwise treated similarly.

444 **PCR to detect a multiple stop codon containing transgene**

445 Genomic DNAs were extracted from LE using the DNAzol RT reagent (Molecular Research
446 Center Inc, Cincinnati, OH), and the concentration and purity determined by spectrophotometry
447 (Nanodrop 1000, Thermo Fisher Scientific Inc., Waltham, MA). The HDR target site(s) on
448 either the 5' or 3' KI transgene was amplified independently with two pairs of primers (Fig 2A):
449 1) 5'KI: 5'int-F and 24nt-6stp-R primers and 2) 3'KI: 24nt-6stp-F and 3'int-R using the GoTaq
450 DNA polymerase mix (Promega, Madison, WI) and 200 nM of each primer. The thermal cycling
451 included denaturation at 95°C, 3 min followed by 30 cycles of 94°C, 30s, 56°C, 30s and 72°C,
452 30s and a final extension for 5 min at 72°C. Thereafter, the amplicons (10 µl) were size separated
453 by agarose gel electrophoresis, stained with ethidium bromide, and imaged using the ChemiDoc
454 Imaging System (Bio-Rad, Hercules, CA). The expected sizes for the 5'KI and 3'KI amplicons
455 were 235 and 182 bp, respectively (Fig 2D). A control PCR to amplify ~790 bp flanking the
456 DSB was included.

457 **Real time qPCR to estimate transgene copy numbers**

458 A SYBR green quantitative PCR-based approach was used to estimate transgene copy numbers
459 using two pairs of primers; 5'KI and 3'KI as detailed (Fig 2A and D) with the SsoAdvanced
460 Universal SYBR Green Supermix (Bio-Rad). Briefly, one ng of gDNA was amplified with 10 µl
461 of 2× SsoAdvanced Universal SYBR Green Supermix and 200 nM of each primer, using the
462 CFX Connect Real-Time PCR Detection System (Bio-Rad). PCR conditions included
463 denaturation at 95°C, 3 min followed by 30 cycles of 94°C, 30 s, 56°C, 30 s and 72°C, 30 s and a
464 final extension at 72°C for 5 min, with the signals collected at the annealing step in each cycle.
465 Analysis of transgene copy number in the pooled gDNAs from LE involved comparison of the
466 qPCR signals obtained using a 10-fold serial dilution series of known quantities of the 24 nt six-
467 stop codon transgene in 235 bp (5' integration PCR fragment) ligated-pCR4-TOPO plasmid
468 DNA (size 4,191 bp) to establish a standard curve (Shirvani *et al*, 2020). The standard curve was
469 based on a linear regression generated using logarithm-10 transformed initial DNA input as the
470 dependent variable and the Ct number of the qPCR signal as the independent variable (Ct values
471 in each dilution were measured in triplicate). Ct numbers were used to fit into the linear
472 regression to derive the estimation of transformed DNA amount for the transgene (Lee *et al*,
473 2006; Yuan *et al*, 2007). The concentration of the 5'KI-transgene ligated-pCR4-TOPO plasmid
474 was measured (NanoDrop 1000) and the corresponding copy number was calculated as follows:

475 $$\text{DNA copy number} = \frac{6.02 \times 10^{23}\ (\text{copy/mol}) \times \text{DNA quantity (g)}}{\text{DNA length (bp)} \times 660\ (\text{g/mol/bp})}$$

477 Data were collected from four biological replicates. 5'KI and 3'KI transgene copy numbers
478 from the *Sp*Cas9 and *As*Cas12a treatments were plotted using GraphPad Prism v9 (Fig 2E and
479 F).

480 **Tracking of INDELs by decomposition (TIDE) analysis**

481 Genomic DNAs from LE exposed to the RNPs were isolated as above. The target *omega-1* locus
482 in the replicates of gDNAs was amplified using a control primer pair (Fig 2A). The amplicon of
483 790 bp in size from control and experimental groups, both KO and KI focused manipulations,
484 was purified by NucleoSpin® Gel and PCR clean up (Macherey-Nagel, Bethlehem, PA) after
485 which the nucleotide sequence determined by the Sanger method (Genewiz, South Plainland,
486 NJ). Sanger sequence traces from the 12 independent replicates of the experimental groups for
487 both *Sp*Cas9 or *As*Cas12a- (Jacobsen *et al.*, 2020) and *Sp*Cas9-catalyzed gene editing
488 manipulations were analyzed and compared with reads from the control (mock) group using the
489 Tracking of Indels by Decomposition (TIDE) algorithm (Brinkman *et al*, 2014; Brinkman & van
490 Steensel, 2019; Meshalkina *et al*, 2020). TIDE provides a rapid and informative assay and also
491 inform decisions on whether proceed to more detailed high throughput, next generation
492 sequencing (NGS) of targeting amplicons (Germini *et al*, 2018).

493 **On-target amplicon next-generation sequencing**

494 Subsequently, the Amplicon-EZ next generation sequencing approach (Genewiz) was used for
495 deeper coverage of the *ω1* coding sequence mutations and provided > 50,000 reads per sample.

496 Amplicons of 426 bp obtained with the primers bearing Illumina partial adapter sequences at the
497 5' end - NGS-F 5'- TATTGTCAACGGCGTACAGG-3' and NGS-R 5'-
498 CAATCGGCACTGAGACGCA-3' - flanking the programmed DSBs for CRISPR/*Sp*Cas9 and
499 CRISPR/*As*Cas12a were sequenced using Illumina chemistry. Partial Illumina adapters were
500 added to 5' end of the forward and reverse primers forward sequencing read: 5'-
501 ACACTCTTTCCCTACACGACGCTCTTCCGATCT-3', reverse sequencing read: 5'-
502 GACTGGAGTTCAGACGTGTGCTCTTCCGATCT-3'. The amplicons were purified using the
503 NucleoSpin® Gel and PCR clean up kits from Macherey-Nagel (Bethlehem, PA), after which
504 quantification and qualification of purified band(s) were undertaken using the Agilent DNA 1000
505 kit and BioAnalyzer (Agilent). Illumina NGS was performed with 2×250 bp sequencing without
506 fragmenting the amplicons. Raw reads in FASTQ format were analyzed for mutations resulting
507 from NHEJ and HDR by CRISPREsso2 (Clement *et al*, 2019) using the reference *ω1* sequences,
508 Smp_334170 and Smp_333930 including Smp_333870 (this latter is annotated as an
509 uncharacterized protein but shares >99% identity) (Fig S1B). The default parameters were used
510 to estimate indel and HDR events. The sequence reads from the Amplicon-EZ runs are available
511 at GenBank Bioproject PRJNA415471, BioSample SAMN07823308, SRA study SRP126685,
512 accessions SRR: 13498338-13498342, 15971309-15971320, and 6374209-6374210.

513 **Quantitative real time PCR**

514 Total RNA of LE was isolated using the RNAzol RT reagent (Molecular Research Center)
515 according to the manufacturer's instruction. RNA concentration and purity were determined
516 (Nanodrop 1000 spectrophotometer, Thermo Fisher). Ten nanograms of RNA was treated with
517 DNase I to remove residual DNA then converted to cDNA by Maxima First Strand cDNA
518 Synthesis Kit (Thermo Fisher Scientific). The *ω1*-specific product was amplified using
519 SsoAdvanced Universal SYBR Green Supermix (Bio-Rad) on CFX96 real time PCR (Bio-Rad)
520 using the primers as described (Ittiprasert *et al.*, 2019), ω1-RT-F: 5'-
521 GGTTACTTTAAATTTGGTA-3' and ω1-RT-R; 5'-AGTTTCCAAGGAACGGGCAG-3'.
522 These primers amplify all annotated *ω1* transcript copies; Smp_334170.1, Smp_334170.2,
523 Smp_334240 and Smp_333930 (Fig S1C). The PCR reaction was denatured at 95°C for 30 s, 40
524 amplification cycles each consisting of denaturation at 95°C for 15 s and annealing/extension at
525 60°C for 30 s. The output was analyzed in CFX manager software (Bio-Rad). Relative
526 expression of ω1 was calculated using the $2^{-\Delta\Delta Ct}$ method and normalized to schistosome GAPDH
527 (Smp_0569701) expression using specific primers; forward 5'-
528 ATGGGACATTTCCAGGCGAG-3', reverse 5'-CCAACAACGAACATGGGTGC-3' (Livak &
529 Schmittgen, 2001). Data four biological replicates were compared to wild type LE and fold
530 change reported as mean ± SE (n = 4).

531 **Western blot analysis**

532 Soluble egg antigen (SEA) of LE was extracted by mechanical lysis (Funakoshi motorized
533 pestle; Diagnocine, Hackensack, NJ) in RIPA buffer (Millipore Sigma) supplemented with
534 protease inhibitors (Protease Inhibitor Cocktail I, Millipore Sigma), as described (Ittiprasert *et*
535 *al.*, 2019). The lysate was clarified by centrifugation at 13,000 rpm, 15 min, 4°C after which
536 protein concentration was determined by the Bradford method (Kielkopf *et al*, 2020). Ten
537 micrograms of SEA were size-separated through SDS-PAGE polyacrylamide gradient gels, 4-
538 12% gel, w/v (Bolt Bis-Tris Plus, Invitrogen, Thermo Fisher Scientific) before transfer to PVDP

539 membranes (Transblot Turbo Transfer System, Bio-Rad). Polyclonal anti-ω1 IgG antibodies
540 were purified from the rabbit anti-ω1 sera, raised as follows. Two NZ white rabbits, E12983 and
541 E12984, were immunized with 30 μg of recombinant *omega-1* RNase T2 of *Schistosoma*
542 *mansoni* (rω1) (produced *in planta* by agroinfiltration of leaves of *Nicotiana benthamiana*
543 (Wilbers *et al*, 2017)) in Complete Freund's Adjuvant and boosted four times at two-week
544 intervals using 15 μg rω1 in Incomplete Freund's Adjuvant each time. Blood was collected 66
545 days after the first immunization, IgGs was isolated from sera using an immobilized protein A
546 ligand. The concentrations of the purified antibodies were 1.31 mg/ml (E12983) and 1.51 mg/ml
547 (E12984). These antibodies have been assigned Research Resource Identifier (RRID)
548 AB_2889886 (Bandrowski *et al*, 2016). PVDF membranes were probed with the E12983 IgG
549 antibody, diluted 1:1,000, for 18 h at 4°C in PBS-Tween (0.5%), 5% non-fat powdered milk,
550 washed 3 times in PBS-Tween (wash buffer), and probed with goat anti-rabbit IgG (H+L) horse
551 radish peroxidase conjugate (Life Technologies, Thermo Fisher Sciences), diluted 1:5,000, for
552 60 min at 23°C with gentle shaking. Subsequently, following washing (3 times in wash buffer),
553 the membrane was exposed to a peroxidase substrate (Clarity Western ECL Substrate, Bio-Rad)
554 for 5 min at 23°C, after which chemiluminescence was quantified and imaged (Chemi-Doc MP
555 System, Bio-Rad). The Image Lab software (Bio-Rad) was used to quantify the ω1 signals. The
556 percentage of ω1 expression from the experimental and control groups was established by
557 comparison with that of wild type SEA, assigned as 100%.

558 **Single stranded DNA donors as a potential substrate for indiscriminate *trans* activity of**
559 **activated** *As*Cas12a

560 Previous reports reveal the *trans*-activity of wild type *As*Cas12a prefers ssDNAs over dsDNAs,
561 and was inactive toward dsDNA in the presence of magnesium (II) ions (Li *et al*, 2020). The
562 *As*Cas12a exhibited not only endonuclease activity on both dsDNA, *cis*- and *trans*-activity (Li *et*
563 *al*, 2018b). Accordingly, to investigate whether activated *As*Cas12a could degrade the ssODN
564 donors used in this study by indiscriminate *trans*-activity, several *in vitro As*Cas12a-RNP
565 digestion assays were carried out. These included the dsDNAs containing the *As*Cas12a target
566 sequence used in this study and 5'PAM (TTTG) as positive enzymatic activity. A 426 bp
567 dsDNA template was amplified using the NGS study (above) primers. Activity of *As*Cas12a-
568 RNP against the dsDNA template released fragments of 265 and 161 bp (Fig 2B), at 37°C for
569 ≥30 min as predicted in 1× NEB Buffer 2.1 (500 mM NaCl, 20 mM sodium acetate, 0.1 mM
570 EDTA, 0.1 mM tris(2-carboxyethyl) phosphine (TCEP), 50% glycerol). *As*Cas12a activity was
571 inactivated by the addition of Proteinase K (1 ul at 20 mg/ml) at 56°C for 10 min.
572 Electropherograms of the digestion products were undertaken using the BioAnalyzer (Agilent
573 DNA1000) to visualize the size templates and fragments.

574 To investigate indiscriminate *trans*-cleavage of ssODNs, similar *in vitro* digestion reaction was
575 carried out, as above, but with the addition of |50 ng of either *As*Cas12a-NT-ssODN or
576 *As*Cas12a-T-ssODN. The *As*Cas12a-RNP complex in 1× NEB Buffer 2.1 and ssODN were
577 incubated at 37°C for 30, 60 and 120 min before stopping the reaction by addition of proteinase
578 K at 56°C for 10 min, as visualized as above. The ssDNA ladder (SimPlex Sciences, NJ)
579 ranging from 10-200 bp was included as the single stranded DNA marker. *Trans*-activity of Alt-
580 R *As*Cas12a V3-RNP complex was not apparent against the ssODNs under these conditions *in*
581 *vitro* (Fig 2C).

582 **Statistical analysis**

583 Statistical analysis was performed using GraphPad Prism version 9.1 (GraphPad Prism, La Jolla,
584 CA). Graphs were plotted as the mean with bars to show the standard error of the mean. The
585 differences among groups were assessed by one-way ANOVA. *P*-values ≤ 0.05 considered to be
586 the statistically significant.

587 **GenBank/EMBL/DDBJ**

588 **Database accessions**

589 Nucleotide sequences reads of the amplicons are available at Bioproject
590 PRJNA415471, https://www.ncbi.nlm.nih.gov/bioproject/PRJNA415471 and GenBank
591 accession PRJNA415471, BioSample, SAMN07823308, SRA, SRP126685.

592 **cknowledgements**

593 We thank Professor Cornelis Hokke, Leiden University Medical Center, The Netherlands for the
594 gift of recombinant *Schistosoma mansoni* omega-1. We thank the Thailand Research Fund, the
595 Royal Golden Jubilee Ph.D. program, and Dr. Dalina Tanyong, Mahidol University, Thailand,
596 for support for CC to perform the work at GWU. This research was funded in whole, or in part,
597 by the Wellcome Trust (award number 107475/Z/15/Z, titled 'Functional Genomics Flatworms
598 Initiative', K. H. Hoffmann, principal investigator). For the purpose of Open Access, the authors
599 have applied a CC BY public copyright license to any Author Accepted Manuscript version
600 arising from this submission. Schistosome-infected mice and snails were provided by the NIAID
601 Schistosomiasis Resource Center of the Biomedical Research Institute, Rockville, Maryland
602 through NIH-NIAID Contract HHSN272201000005I for distribution through BEI Resources.

603 **Author contributions**.

604 WI, CC, and PJB designed the experiments, analyzed the data, and drafted the manuscript with
605 input from all the co-authors; CC and WI performed the gene editing focused experiments;
606 VHM, WL, AM, TO, YNA and MMK contributed the parasite materials to the experiments, to
607 data collection, and reviewed and edited the manuscript; PJB and WI supervised the project.
608 PJB, WI and MMK arranged the funding.

609 **Conflict of interest**

610 The authors declare that do not have competing interests**.**

611 **Figure legends**

612 **Figure 1. Schematic of the *S. mansoni* hepatotoxic ribonuclease omega 1 (ω1) gene**
613 **structure, target sites for the *Sp*Cas9 and *As*Cas12a, ssODN donors and partial amino acid**
614 **sequence with histidine active site.**

615 A Diagram of the ω1 gene (Gene ID; Smp_334170.2 of *S. mansoni* annotated genome version
616 7_2021) and CRISPR/Cas target sites on coding sequencing of the first exon coding for

617 histidine active site, FRKHEFEKHGLCAVEDPQV. The relative positions of crRNA for
618 CRISPR-*Sp*Cas9 (red arrow) and -*As*Cas12a (blue arrow) are indicated along with their
619 3'PAM (yellow arrow) and 5'PAM (yellow arrow), respectively.

620 B Programmed cleavage site for *Sp*Cas9/sgRNA ~3nt upstream of PAM 3'TGG (red arrow);
621 and cleavage site for *As*Cas12a/crRNA at 18-24 nt downstream of a prospective 5-'TTTV)
622 (blue arrow). The programmed cleavage sites for both enzymes, *Sp*Cas9 and *As*Cas12a,
623 were three to six nt distant from each other. Fifty residues upstream and downstream of the
624 double strand break (DSB) were included as the homology arms (HA) of the six stop codon
625 cassette transgene (payload/cargo). Because cleavage by *Sp*Cas9 liberates blunt ended
626 DNA, only a non-target strand (NT) repair template was provided for HDR (red bar). Sticky
627 ended DNA results from cleavage by *As*Cas12a and hence both non target and target strand
628 (T) repair templates for HDR were provided (light and dark blue bars).

629 C The DNA donor sequences of CRISPR/*Sp*Cas9 and CRISPR/*As*Cas12a with non-target
630 (NT) or target (T) sequence HA where the *As*Cas12a-NT-ssODN donor repairs the anti-
631 sense DNA and *As*Cas12a-T-ssODN donor repairs the sense stand.

632 **Figure 2. Knock-in by homology directed repair.**

633 A The location of primers used for 5'- and 3' transgene (purple lines) knock-in PCR (5'int-F
634 with 24nt-6stp-R and 24nt-6stp-F with 3'int-R) and internal positive control (control-F and
635 -R). The primers for next generation sequencing indicate as NGS-F and NGS-R. All
636 primers locates further from HA (purple boxes) to protect the false positive PCR from
637 DNA donor and 24 nt-6stp-F and -R primers are highly specific to stop codon transgene,
638 not schistosome genome.

639 B The *As*Cas12a target recognition activates specific 426 bp dsDNA amplicon template (lane
640 1) cleavage into 265bp and 161 bp (lane 3). The crRNA/*As*Cas12a RNP complex is ~40 nt
641 are in lanes 2 and 3.

642 C There were no specific ssDNA cleavage on either *As*Cas12a-NT-ssODN or *As*Cas12a-T-
643 ssODN donors at 124 nt as in lanes 1 and 2, respectively. The crRNA/*As*Cas12a RNP (~40
644 nt in lanes 3-9) containing activated *As*Cas12a enzyme shown no random ssDNA digestion
645 at 30 min, 60 and 120 min in lanes 4-5, 6-7 and 8-9, respectively. Lanes 4, 6 and 8 shown
646 the uncut 124 nt of *As*Cas12a-NT-ssODN (top band) with *As*Cas12a-crRNA (lower band),
647 and lanes 5, 7 and 9 shows 124 nt of *As*Cas12a-T-ssODN (top band) with *As*Cas12a-
648 crRNA (lower band).

649 D The PCR detection of the integration sites in the transgenic eggs and control. The
650 amplified control product (lanes C) for the wildtype sequence was 790 bp, while those for
651 the 5'(lanes 5') and 3' (lanes 3') flanking regions of the transgenic sequence were 235 bp
652 and 182 bp from KI introducing CAS-9 ssODN, *As*Cas12a-NT-ssODN and *As*Cas12a-T-
653 ssODN, respectively. Lane M is a 1 kb Plus DNA ladder; Mock (only buffer
654 electroporation) used as the negative transgene integration control.

655 E and F The estimation of transgene copy number analysis in egg DNA were calculated by
656 qPCR comparing with the known amount of 24 nt transgene in 235 bp (5' integration PCR

657 fragment) ligated-pCR4-TOPO plasmid DNA (size 4,191 bp) standard curve; y = -
658 4.0964ln(10) + 44.821, R^2 = 0.9923 (data not shown). There were the confirmation of 3'
659 integration of 3.61±0.25, 4.44±0.84 and 4.19±1.22 of transgene copy from KI_*Sp*Cas9,
660 KI_*As*Cas12a-NT-ssODN and KI_*As*Cas12a-T-ssODN, respectively with no statistic
661 significant (one-way ANOVA, multiple comparisons, 95% CI of diff, P Value at 0.4057,
662 0.6264 and 0.9155). While there was asymmetric HDR revealed by 5' transgene integration
663 of 2.72±0.42, 5.06±0.54 and 1.64±0.39 copy number from KI_*Sp*Cas9, KI_*As*Cas12a-NT-
664 ssODN and KI_*As*Cas12a-T-ssODN, respectively. The asterisk *,*** and **** indicates
665 statistic significant difference with P = 0.0214, P=0.0001 and P < 0.0001, respectively by
666 one-way ANOVA, multiple comparison. The control primers used for amplicon
667 preparation from both control and experimental groups, then their Sanger Direct
668 Sequencing results were pre-investigated for CRISPR efficiency by TIDE analysis prior to
669 proceed for NGS.

670 G and H 5'int-F and 3'int-R are genome-specific primers, and 24nt-6stp-F and 24nt-6stp-R
671 are transgene-specific primers. From these results, we confirmed that programmed
672 CRISPR/*As*Cas12a gene editing was active in schistosome eggs, and higher than *Sp*Cas9 by
673 TIDE analysis with statistic significant (ANOVA, ****, P 0.0001, n = 12). The estimation
674 of CRISPR efficiency from the 12 biological replicates (each black dot in panels G and H)
675 KI_*Sp*Cas9 experiment (wide range of CRISPR efficiency from 0.46-2.23 among 12
676 biological replicates) was higher than KO experiment. The estimated CRISPR efficiency
677 in LE from CRISPR/*As*Cas12a (green dots in panels G and H, n = 8) shown more than
678 1.5% in most samples. There was no statistically significant differences in CRISPR
679 efficiency among KI_*Sp*Cas9 vs. KI_*As*Cas12a (panel H) from Sanger sequencing along
680 with TIDE analysis. Samples of the genomic DNAs were pooled, targeted amplicons
681 prepared, and Illumina NGS performed.

682 **Figure 3. NHEJ assessment from *S. mansoni* eggs on target ω1 gene after *Sp*Cas9 and**
683 ***As*Cas12a RNP complex electroporation.** CRISPResso2 analysis of the Illumina sequence
684 reads revealed non-homologous end joining mutations at targeted loci in schistosome eggs.
685 Allele-specific editing outcomes of CRISPR-*Sp*Cas9 and -*As*Cas12a gene editing in schistosome
686 multiple copies of *ω1* Smp_334170.2, Smp_334170.1, Smp_334240 (100% gene sequence
687 identical; Fig. S1b). Mutagenesis frequencies for all loci including Smp_333930 and
688 Smp_333870 were included in CRISPResso2 analysis (Fig S1B). The results were from NGS
689 libraries of pooled genomic DNA from 7 biological replicates of ω1 gene editing experiments of
690 KO-*Sp*Cas9 (Panel A and C) and KO-*As*Cas12a (Panel B and D). The sequence reads assigned
691 to references, Smp_333930 and Smp_333870 loci by the software to achieve accurate
692 quantification of genome editing at genomic loci with multiple copies from *Sp*Cas9 and
693 *As*Cas12a. The bar chart shows the assignment of each read to the wild type (unmodified) and
694 NHEJ with 12.26%, 1.66% and 0.12% (total 14.04%) from Δω1KO-*Sp*Cas9 on references and
695 other two loci, respectively (panel a). Panel b shows the assigned NHEJ with 9.27%, 1.33% and
696 0.28% (total 10.88%) from Δω1-*As*Cas12a on references and two high identity of *ω1* gene loci
697 (panel b). Ambiguous aligments; 0.49% and 0.93% that could not be attributed uniquely to one
698 of these loci are shown in the last bar of each graph. The majority of NHEJ indels from both
699 nucleases were nucleotide substitutions followed by gene deletions (Panel C and D) on the
700 references. The mutations occurred in all ω1 gene copies with the most editing on the reference
701 target site. CRISPResso2 software interpreted ≤ 1.0% of the reads as ambiguous. Only deletions

702 were revealed in these experiment, -3 nt deletion downstream from expected cut side (red arrow)
703 was the majority of NHEJ mediated from *Sp*Cas9 (Panel C). The larger deletion from -2 to -26
704 nt at downstream of expected sticky end cut sites (red arrows) were revealed from NHEJ.

705 **Figure. 4. HDR and induction of NHEJ at the ω1 target sites using ssODN template.** Panel
706 A to C shown the percentage of NHEJ from egg samples that introduced RNP along with ssODN
707 template were higher than without ssODN. There were total 15.67% (13.22+1.16+0.52), 28.71%
708 (22.31+6.17+0.23) and 21.43% (9.62+11.56+0.25) from Δω1KI-*Sp*Cas9, Δω1KI-*As*Cas12a-NT-
709 ssODN and Δω1KI-*As*Cas12a-T-ssODN, respectively (blue or green bars in each graph).
710 Majority of mutations are substitutions and deletions toward to downstream of the expected cut
711 sites indicating by red arrows (Panel D, E and F). The various base deletions from -1 to -15 bp
712 found in Δω1KI-*Sp*Cas9, Δω1KI-*As*Cas12a-NT-ssODN egg DNAs, while large deletion as -40
713 bp found as a major deletion in Δω1KI-*As*Cas12a-T-ssODN. The percentage of perfect HDR in
714 3 experimental groups; Δω1KI-*Sp*Cas9, Δω1KI-*As*Cas12a-NT-ssODN and Δω1KI-*As*Cas12a-T-
715 ssODN were 17.07%, 14.58% and 12.37%, respectively (red bars, Panel G, H and I). The
716 imperfect HDRs occurred in all KI samples resulting from interrupting 5' end HDR gene repair
717 with 2-5 nucleotide base missing (black bars in Panel G, H and I) with small percentage at 0.94,
718 0.41 and 0.68.

719 **Figure 5. Reduction of the expression of ω1 by quantitative real time PCR and immunoblot**
720 **analysis.**

721 A Reduction of ω1 transcript from Δω1KO-*Sp*Cas9, Δω1KI-*Sp*Cas9, Δω1KO-*As*Cas12a,
722 Δω1KI-*As*Cas12a NTS and Δω1KI-*As*Cas12a TS eggs comparing with control groups after
723 normalization with wild type egg RNA (100% as discontinued line). The means of four
724 independent biological replicates.

725 B and C Soluble egg antigen; SEA (in duplicates) was solubilized, electrophoresed in
726 SDS-PAGE gels, transferred to nitrocellulose membrane, and probed with anti-recombinant
727 plant omega-1 (rω1) rabbit IgG. There was ω1 protein reduction in all SEA samples (~30
728 kDa as arrow, Panel B). The percentage of ω1 expression in both KO and KI experimental
729 samples were comparing ω1 amount of wild-type SEA (100%) (Panel C); (one-way
730 ANOVA, multiple comparison, *, $P< 0.05$, ***, $P< 0.001$, ****, $P<0.0001$).

731 **Supporting information**

732 **Figure S1**. **Gene structure encoding the hepatotoxic ribonuclease, omega 1 (ω1). At least**
733 **five copies of the gene are located on chromosome 1, as apparent in the draft sequence of *S.***
734 ***mansoni*, version 7, scaffold SM_V7_1:3,885,722-4,002,365.** The positions of several ω1
735 genes coding on updated annotation (year 2021) on WormBase Parasite, including two loci of
736 Smp_334170, Smp_334240, Smp_334070, Smp_3332220, Smp_333930, Smp_333870 and
737 Smp_179960 are shown for their physical relationship of the copies on the chromosome.

738 A Map of gene structures and sizes of Smp_334170.1, Smp_334170.2 and Smp_334240 and
739 the CRISPR/Cas programmed target sites for *Sp*Cas9 (blue arrow) and *As*Cas12a (green
740 arrow).

741 B All gene copies shown DNA sequence identity >99% as DNA sequence alignment and
742 target amplicon primer indicated as NGS-F and NGS-R. Only four of these gene copies;
743 Smp_334240, Smp_334170 and Smp_333930 were reported for Uniprot.

744 C Alignment of mRNA sequences and primers used for gene transcript study (purple).

745 **Table S1.** The CRISPREsso2 analysis results from four negative controls; mixed sgRNAs only,
746 *Sp*Cas9 only, *As*Cas12a only and mixed donors only. There were over 180,000 reads from each
747 library. There was < 1% of background modified reads from all negative control samples.

748 **Table S2.** Nucleotide sequences of oligonucleotide primers used in the investigation.

749

750 **References**

751 An Y, Geng Y, Yao J, Fu C, Lu M, Wang C, Du J (2020) Efficient Genome Editing in Populus
752 Using CRISPR/Cas12a. *Front Plant Sci* 11: 593938

753 Arunsan P, Ittiprasert W, Smout MJ, Cochran CJ, Mann VH, Chaiyadet S, Karinshak SE, Sripa
754 B, Young ND, Sotillo J *et al* (2019) Programmed knockout mutation of liver fluke granulin
755 attenuates virulence of infection-induced hepatobiliary morbidity. *Elife* 8

756 Banakar R, Schubert M, Collingwood M, Vakulskas C, Eggenberger AL, Wang K (2020)
757 Comparison of CRISPR-Cas9/Cas12a Ribonucleoprotein Complexes for Genome Editing
758 Efficiency in the Rice Phytoene Desaturase (OsPDS) Gene. *Rice* 13: 4

759 Bandrowski A, Brush M, Grethe JS, Haendel MA, Kennedy DN, Hill S, Hof PR, Martone ME,
760 Pols M, Tan SC *et al* (2016) The Resource Identification Initiative: a cultural shift in publishing.
761 *Brain Behav* 6: e00417

762 Bolt BJ, Rodgers FH, Shafie M, Kersey PJ, Berriman M, Howe KL (2018) Using WormBase
763 ParaSite: An Integrated Platform for Exploring Helminth Genomic Data. *Methods Mol Biol*
764 1757: 471-491

765 Brinkman EK, Chen T, Amendola M, van Steensel B (2014) Easy quantitative assessment of
766 genome editing by sequence trace decomposition. *Nucleic Acids Res* 42: e168

767 Brinkman EK, van Steensel B (2019) Rapid Quantitative Evaluation of CRISPR Genome Editing
768 by TIDE and TIDER. *Methods Mol Biol* 1961: 29-44

769 Charpentier E (2015) CRISPR-Cas9: how research on a bacterial RNA-guided mechanism
770 opened new perspectives in biotechnology and biomedicine. *EMBO Mol Med* 7: 363-365

771 Charpentier E, Richter H, van der Oost J, White MF (2015) Biogenesis pathways of RNA guides
772 in archaeal and bacterial CRISPR-Cas adaptive immunity. *FEMS Microbiol Rev* 39: 428-441

773 Chen JS, Ma E, Harrington LB, Da Costa M, Tian X, Palefsky JM, Doudna JA (2018) CRISPR-
774 Cas12a target binding unleashes indiscriminate single-stranded DNase activity. *Science* 360:
775 436-439

776 Clement K, Rees H, Canver MC, Gehrke JM, Farouni R, Hsu JY, Cole MA, Liu DR, Joung JK,
777 Bauer DE *et al* (2019) CRISPResso2 provides accurate and rapid genome editing sequence
778 analysis. *Nat Biotechnol* 37: 224-226

779 Costain AH, MacDonald AS, Smits HH (2018) Schistosome Egg Migration: Mechanisms,
780 Pathogenesis and Host Immune Responses. *Front Immunol* 9: 3042

781 Dalton JP, Day SR, Drew AC, Brindley PJ (1997) A method for the isolation of schistosome
782 eggs and miracidia free of contaminating host tissues. *Parasitology* 115 (Pt 1): 29-32

783 Dumeau CE, Monfort A, Kissling L, Swarts DC, Jinek M, Wutz A (2019) Introducing gene
784 deletions by mouse zygote electroporation of Cas12a/Cpf1. *Transgenic Res* 28: 525-535

785 Everts B, Perona-Wright G, Smits HH, Hokke CH, van der Ham AJ, Fitzsimmons CM, Doenhoff
786 MJ, van der Bosch J, Mohrs K, Haas H *et al* (2009) Omega-1, a glycoprotein secreted by
787 Schistosoma mansoni eggs, drives Th2 responses. *J Exp Med* 206: 1673-1680

788 Fuchs RT, Curcuru J, Mabuchi M, Yourik P, Robb GB (2019) Cas12a trans-cleavage can be
789 modulated in vitro and is active on ssDNA, dsDNA, and RNA. *bioRxiv*: 600890

790 Germini D, Tsfasman T, Zakharova VV, Sjakste N, Lipinski M, Vassetzky Y (2018) A
791 Comparison of Techniques to Evaluate the Effectiveness of Genome Editing. *Trends Biotechnol*
792 36: 147-159

793 Gier RA, Budinich KA, Evitt NH, Cao Z, Freilich ES, Chen Q, Qi J, Lan Y, Kohli RM, Shi J
794 (2020) High-performance CRISPR-Cas12a genome editing for combinatorial genetic screening.
795 *Nat Commun* 11: 3455

796 Hendel A, Bak RO, Clark JT, Kennedy AB, Ryan DE, Roy S, Steinfeld I, Lunstad BD, Kaiser
797 RJ, Wilkens AB *et al* (2015) Chemically modified guide RNAs enhance CRISPR-Cas genome
798 editing in human primary cells. *Nat Biotechnol* 33: 985-989

799 Hoffmann KF, Brindley PJ, Berriman M (2014) Medicine. Halting harmful helminths. *Science*
800 346: 168-169

801 Hsu PD, Lander ES, Zhang F (2014) Development and applications of CRISPR-Cas9 for
802 genome engineering. *Cell* 157: 1262-1278

803 Huang CH, Lee KC, Doudna JA (2018) Applications of CRISPR-Cas Enzymes in Cancer
804 Therapeutics and Detection. *Trends Cancer* 4: 499-512

805 Hur JK, Kim K, Been KW, Baek G, Ye S, Hur JW, Ryu SM, Lee YS, Kim JS (2016) Targeted
806 mutagenesis in mice by electroporation of Cpf1 ribonucleoproteins. *Nat Biotechnol* 34: 807-808

807 International Helminth Genomes C (2019) Comparative genomics of the major parasitic worms.
808 *Nat Genet* 51: 163-174

809 Ittiprasert W, Mann VH, Karinshak SE, Coghlan A, Rinaldi G, Sankaranarayanan G, Chaidee A,
810 Tanno T, Kumkhaek C, Prangtaworn P *et al* (2019) Programmed genome editing of the omega-1
811 ribonuclease of the blood fluke, Schistosoma mansoni. *Elife* 8

812 Jacobsen T, Ttofali F, Liao C, Manchalu S, Gray BN, Beisel CL (2020) Characterization of
813 Cas12a nucleases reveals diverse PAM profiles between closely-related orthologs. *Nucleic Acids*
814 *Res* 48: 5624-5638

815 Jeon Y, Choi YH, Jang Y, Yu J, Goo J, Lee G, Jeong YK, Lee SH, Kim IS, Kim JS *et al* (2018)
816 Direct observation of DNA target searching and cleavage by CRISPR-Cas12a. *Nat Commun* 9:
817 2777

818 Jinek M, Chylinski K, Fonfara I, Hauer M, Doudna JA, Charpentier E (2012) A programmable
819 dual-RNA-guided DNA endonuclease in adaptive bacterial immunity. *Science* 337: 816-821

820 Jurberg AD, Goncalves T, Costa TA, de Mattos AC, Pascarelli BM, de Manso PP, Ribeiro-Alves
821 M, Pelajo-Machado M, Peralta JM, Coelho PM *et al* (2009) The embryonic development of
822 Schistosoma mansoni eggs: proposal for a new staging system. *Dev Genes Evol* 219: 219-234

823 Kellner MJ, Koob JG, Gootenberg JS, Abudayyeh OO, Zhang F (2019) SHERLOCK: nucleic
824 acid detection with CRISPR nucleases. *Nat Protoc* 14: 2986-3012

825 Kielkopf CL, Bauer W, Urbatsch IL (2020) Bradford Assay for Determining Protein
826 Concentration. *Cold Spring Harb Protoc* 2020: 102269

827 Kim D, Kim J, Hur JK, Been KW, Yoon SH, Kim JS (2016) Genome-wide analysis reveals
828 specificities of Cpf1 endonucleases in human cells. *Nat Biotechnol* 34: 863-868

829 Kissling L, Monfort A, Swarts DC, Wutz A, Jinek M (2019) Preparation and electroporation of
830 Cas12a/Cpf1-guide RNA complexes for introducing large gene deletions in mouse embryonic
831 stem cells. *Methods Enzymol* 616: 241-263

832 Koonin EV, Makarova KS, Wolf YI (2017) Evolutionary Genomics of Defense Systems in
833 Archaea and Bacteria. *Annu Rev Microbiol* 71: 233-261

834 Labun K, Montague TG, Gagnon JA, Thyme SB, Valen E (2016) CHOPCHOP v2: a web tool
835 for the next generation of CRISPR genome engineering. *Nucleic Acids Res* 44: W272-276

836 Labun K, Montague TG, Krause M, Torres Cleuren YN, Tjeldnes H, Valen E (2019)
837 CHOPCHOP v3: expanding the CRISPR web toolbox beyond genome editing. *Nucleic Acids*
838 *Res* 47: W171-W174

839 Lee C, Kim J, Shin SG, Hwang S (2006) Absolute and relative QPCR quantification of plasmid
840 copy number in Escherichia coli. *J Biotechnol* 123: 273-280

841 Li B, Yan J, Zhang Y, Li W, Zeng C, Zhao W, Hou X, Zhang C, Dong Y (2020) CRISPR-
842 Cas12a Possesses Unconventional DNase Activity that Can Be Inactivated by Synthetic
843 Oligonucleotides. *Mol Ther Nucleic Acids* 19: 1043-1052

844 Li S-Y, Cheng Q-X, Wang J-M, Li X-Y, Zhang Z-L, Gao S, Cao R-B, Zhao G-P, Wang J
845 (2018a) CRISPR-Cas12a-assisted nucleic acid detection. *Cell Discovery* 4: 20

846 Li SY, Cheng QX, Liu JK, Nie XQ, Zhao GP, Wang J (2018b) CRISPR-Cas12a has both cis-
847 and trans-cleavage activities on single-stranded DNA. *Cell Res* 28: 491-493

848 Liu P, Luk K, Shin M, Idrizi F, Kwok S, Roscoe B, Mintzer E, Suresh S, Morrison K, Frazão JB
849 *et al* (2019) Enhanced Cas12a editing in mammalian cells and zebrafish. *Nucleic Acids Res* 47:
850 4169-4180

851 Liu Y, Han J, Chen Z, Wu H, Dong H, Nie G (2017) Engineering cell signaling using tunable
852 CRISPR-Cpf1-based transcription factors. *Nat Commun* 8: 2095

853 Livak KJ, Schmittgen TD (2001) Analysis of relative gene expression data using real-time
854 quantitative PCR and the 2(-Delta Delta C(T)) Method. *Methods* 25: 402-408

855 Lu Z, Sankaranarayanan G, Rawlinson KA, Offord V, Brindley PJ, Berriman M, Rinaldi G
856 (2021) The Transcriptome of Schistosoma mansoni Developing Eggs Reveals Key Mediators in
857 Pathogenesis and Life Cycle Propagation. *Frontiers in Tropical Diseases* 2

858 Luhtala N, Parker R (2010) T2 Family ribonucleases: ancient enzymes with diverse roles. *Trends*
859 *Biochem Sci* 35: 253-259

860 Ma P, Meng Q, Sun B, Zhao B, Dang L, Zhong M, Liu S, Xu H, Mei H, Liu J *et al* (2020)
861 MeCas12a, a Highly Sensitive and Specific System for COVID-19 Detection. *Advanced Science*
862 7: 2001300

863 Malzahn AA, Tang X, Lee K, Ren Q, Sretenovic S, Zhang Y, Chen H, Kang M, Bao Y, Zheng X
864 *et al* (2019) Application of CRISPR-Cas12a temperature sensitivity for improved genome
865 editing in rice, maize, and Arabidopsis. *BMC Biol* 17: 9

866 Mann VH, Morales ME, Rinaldi G, Brindley PJ (2010) Culture for genetic manipulation of
867 developmental stages of Schistosoma mansoni. *Parasitology* 137: 451-462

868 Mann VH, Suttiprapa S, Skinner DE, Brindley PJ, Rinaldi G (2014) Pseudotyped murine
869 leukemia virus for schistosome transgenesis: approaches, methods and perspectives. *Transgenic*
870 *Res* 23: 539-556

871 Meshalkina DA, Glushchenko AS, Kysil EV, Mizgirev IV, Frolov A (2020) SpCas9- and
872 LbCas12a-Mediated DNA Editing Produce Different Gene Knockout Outcomes in Zebrafish
873 Embryos. *Genes (Basel)* 11

874 Montague TG, Cruz JM, Gagnon JA, Church GM, Valen E (2014) CHOPCHOP: a
875 CRISPR/Cas9 and TALEN web tool for genome editing. *Nucleic Acids Res* 42: W401-407

876 Mustafa MI, Makhawi AM (2020) SHERLOCK and DETECTR: CRISPR-Cas Systems as
877 Potential Rapid Diagnostic Tools for Emerging Infectious Diseases. *J Clin Microbiol*

878 Nguyen LT, Smith BM, Jain PK (2020) Enhancement of trans-cleavage activity of Cas12a with
879 engineered crRNA enables amplified nucleic acid detection. *Nature Communications* 11: 4906

880 Nguyen PQ, Soenksen LR, Donghia NM, Angenent-Mari NM, de Puig H, Huang A, Lee R,
881 Slomovic S, Galbersanini T, Lansberry G *et al* (2021) Wearable materials with embedded
882 synthetic biology sensors for biomolecule detection. *Nat Biotechnol*

883 Nishimasu H, Ran FA, Hsu PD, Konermann S, Shehata SI, Dohmae N, Ishitani R, Zhang F,
884 Nureki O (2014) Crystal structure of Cas9 in complex with guide RNA and target DNA. *Cell*
885 156: 935-949

886 Paix A, Folkmann A, Goldman DH, Kulaga H, Grzelak MJ, Rasoloson D, Paidemarry S, Green
887 R, Reed RR, Seydoux G (2017) Precision genome editing using synthesis-dependent repair of
888 Cas9-induced DNA breaks. *Proc Natl Acad Sci U S A* 114: E10745-e10754

889 Pinello L, Canver MC, Hoban MD, Orkin SH, Kohn DB, Bauer DE, Yuan GC (2016) Analyzing
890 CRISPR genome-editing experiments with CRISPResso. *Nat Biotechnol* 34: 695-697

891 Protasio AV, Tsai IJ, Babbage A, Nichol S, Hunt M, Aslett MA, De Silva N, Velarde GS,
892 Anderson TJ, Clark RC *et al* (2012) A systematically improved high quality genome and
893 transcriptome of the human blood fluke Schistosoma mansoni. *PLoS Negl Trop Dis* 6: e1455

894 Ranawakage DC, Okada K, Sugio K, Kawaguchi Y, Kuninobu-Bonkohara Y, Takada T,
895 Kamachi Y (2020) Efficient CRISPR-Cas9-Mediated Knock-In of Composite Tags in Zebrafish
896 Using Long ssDNA as a Donor. *Front Cell Dev Biol* 8: 598634

897 Sankaranarayanan G, Berriman M, Rinaldi G (2021) An uneven race: genome editing for
898 parasitic worms. *Nat Rev Microbiol* 19: 621

899 Santos L, Mention K, Cavusoglu-Doran K, Sanz DJ, Bacalhau M, Lopes-Pacheco M, Harrison
900 PT, Farinha CM (2021) Comparison of Cas9 and Cas12a CRISPR editing methods to correct the
901 W1282X-CFTR mutation. *J Cyst Fibros*

902 Schwartz C, Fallon PG (2018) Schistosoma "Eggs-Iting" the Host: Granuloma Formation and
903 Egg Excretion. *Front Immunol* 9: 2492

904 Sentmanat MF, Peters ST, Florian CP, Connelly JP, Pruett-Miller SM (2018) A Survey of
905 Validation Strategies for CRISPR-Cas9 Editing. *Sci Rep* 8: 888

906 Shirvani R, Barshan-Tashnizi M, Shahali M (2020) An investigation into gene copy number
907 determination in transgenic yeast; The importance of selecting a reliable real-time PCR standard.
908 *Biologicals* 65: 10-17

909 Smith CW, Nandu N, Kachwala MJ, Chen YS, Uyar TB, Yigit MV (2020) Probing CRISPR-
910 Cas12a Nuclease Activity Using Double-Stranded DNA-Templated Fluorescent Substrates.
911 *Biochemistry* 59: 1474-1481

912 Steinfelder S, Andersen JF, Cannons JL, Feng CG, Joshi M, Dwyer D, Caspar P, Schwartzberg
913 PL, Sher A, Jankovic D (2009) The major component in schistosome eggs responsible for
914 conditioning dendritic cells for Th2 polarization is a T2 ribonuclease (omega-1). *J Exp Med* 206:
915 1681-1690

916 Straume AH, Kjaerner-Semb E, Ove Skaftnesmo K, Guralp H, Kleppe L, Wargelius A,
917 Edvardsen RB (2020) Indel locations are determined by template polarity in highly efficient in
918 vivo CRISPR/Cas9-mediated HDR in Atlantic salmon. *Sci Rep* 10: 409

919 Swarts DC (2019) Making the cut(s): how Cas12a cleaves target and non-target DNA. *Biochem*
920 *Soc Trans* 47: 1499-1510

921 Swarts DC, Jinek M (2018) Cas9 versus Cas12a/Cpf1: Structure-function comparisons and
922 implications for genome editing. *Wiley Interdiscip Rev RNA*: e1481

923 Swarts DC, Jinek M (2019) Mechanistic Insights into the cis- and trans-Acting DNase Activities
924 of Cas12a. *Mol Cell* 73: 589-600 e584

925 Takaki KK, Rinaldi G, Berriman M, Pagan AJ, Ramakrishnan L (2021a) Schistosoma mansoni
926 Eggs Modulate the Timing of Granuloma Formation to Promote Transmission. *Cell Host*
927 *Microbe* 29: 58-67 e55

928 Takaki KK, Roca FJ, Schramm G, Wilbers RHP, Ittiprasert W, Brindley PJ, Rinaldi G, Berriman
929 M, Ramakrishnan L, Pagan AJ (2021b) Tumor Necrosis Factor and Schistosoma mansoni egg
930 antigen omega-1 shape distinct aspects of the early egg-induced granulomatous response. *PLoS*
931 *Negl Trop Dis* 15: e0008814

932 Tóth E, Czene BC, Kulcsár PI, Krausz SL, Tálas A, Nyeste A, Varga É, Huszár K, Weinhardt N,
933 Ligeti Z *et al* (2018) Mb- and FnCpf1 nucleases are active in mammalian cells: activities and
934 PAM preferences of four wild-type Cpf1 nucleases and of their altered PAM specificity variants.
935 *Nucleic Acids Res* 46: 10272-10285

936 Wilbers RH, Westerhof LB, van Noort K, Obieglo K, Driessen NN, Everts B, Gringhuis SI,
937 Schramm G, Goverse A, Smant G *et al* (2017) Production and glyco-engineering of
938 immunomodulatory helminth glycoproteins in plants. *Sci Rep* 7: 45910

939 Yuan JS, Burris J, Stewart NR, Mentewab A, Stewart CN, Jr. (2007) Statistical tools for
940 transgene copy number estimation based on real-time PCR. *BMC Bioinformatics* 8 Suppl 7: S6

941 Zamanian M, Andersen EC (2016) Prospects and challenges of CRISPR/Cas genome editing for
942 the study and control of neglected vector-borne nematode diseases. *Febs j* 283: 3204-3221

943 Zetsche B, Gootenberg JS, Abudayyeh OO, Slaymaker IM, Makarova KS, Essletzbichler P, Volz
944 SE, Joung J, van der Oost J, Regev A *et al* (2015) Cpf1 is a single RNA-guided endonuclease of
945 a class 2 CRISPR-Cas system. *Cell* 163: 759-771

946 Zhang Y, Ren Q, Tang X, Liu S, Malzahn AA, Zhou J, Wang J, Yin D, Pan C, Yuan M *et al*
947 (2021) Expanding the scope of plant genome engineering with Cas12a orthologs and highly
948 multiplexable editing systems. *Nat Commun* 12: 1944

figure 1

A

B

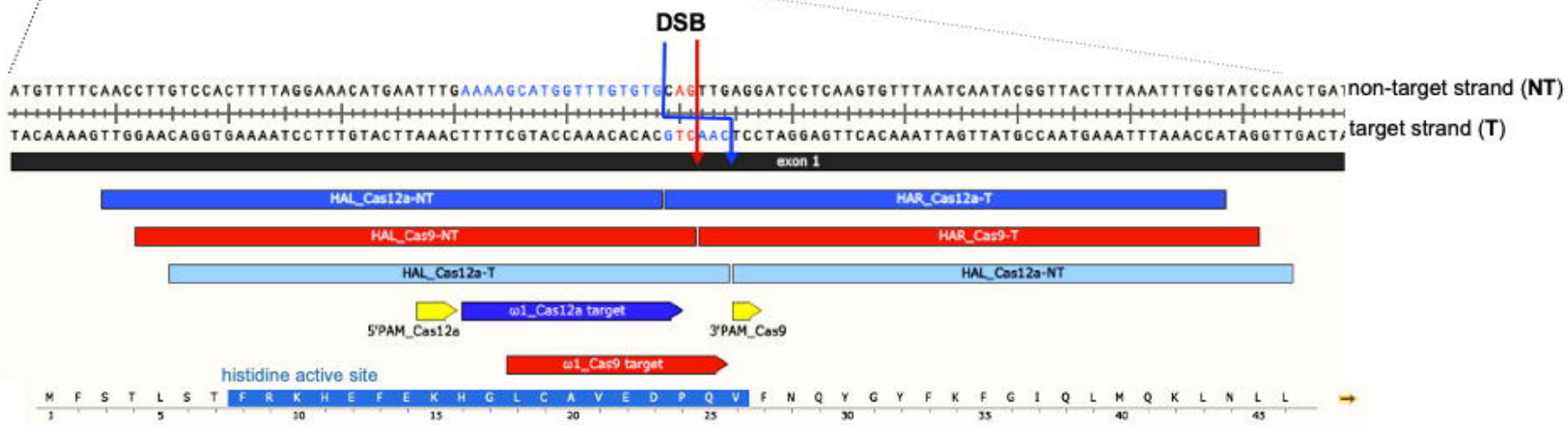

C

Cas9-ssODN:

cttgtccacttttaggaaacatgaatttgaaaagcatggtttgtgtgcagTAAGTGACTAGGTAACTGAGTAGCttgaggatcctcaagtgtttaatcaatacggttactttaaatttggtatt

Cas12a- NT-ssODN:

tgtccacttttaggaaacatgaatttgaaaagcatggtttgtgtgcagttTAAGTGACTAGGTAACTGAGTAGCgaggatcctcaagtgtttaatcaatacggttactttaaatttggtattaa

Cas12a- T-ssODN:

attggaacaggtgaaaatcctttgtacttaaacttttcgtaccaaacacacATTCACTGATCCATTGACTCATCGgtcaactcctaggagttcacaaattagttatgccaatgaaatttaaacca

figure 2

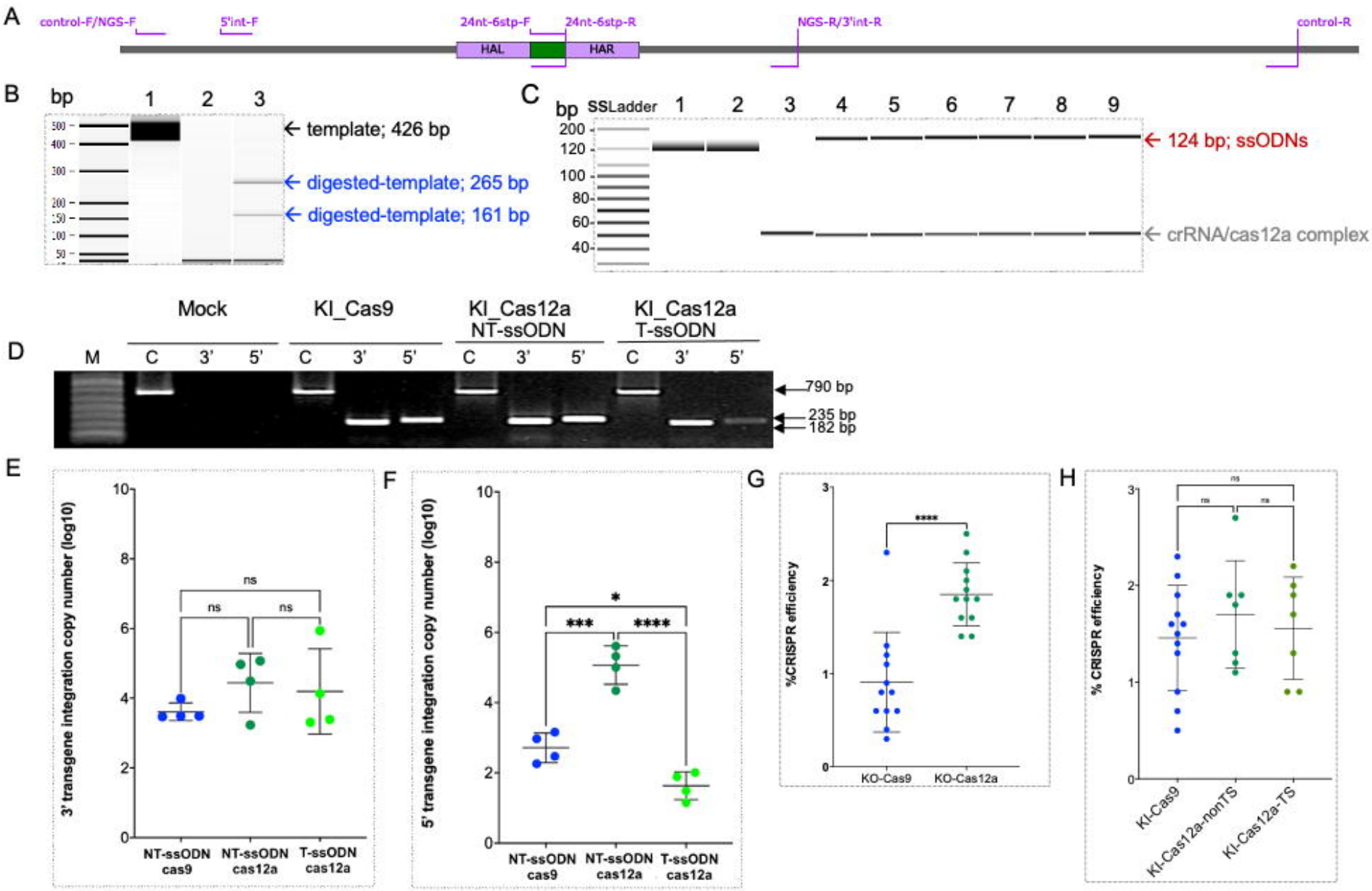
A
control-F/NGS-F
5'int-F
24nt-6stp-F
24nt-6stp-R
NGS-R/3'int-R
control-R
HAL
HAR
B
bp
1
2
3
500
400
300
200
150
100
50
template; 426 bp
digested-template; 265 bp
digested-template; 161 bp
C
bp
SSLadder
1
2
3
4
5
6
7
8
9
200
120
100
80
60
40
124 bp; ssODNs
crRNA/cas12a complex
D
Mock
KI_Cas9
KI_Cas12a NT-ssODN
KI_Cas12a T-ssODN
M
C
3'
5'
790 bp
235 bp
182 bp
E
3' transgene integration copy number (log10)
ns
NT-ssODN cas9
NT-ssODN cas12a
T-ssODN cas12a
F
5' transgene integration copy number (log10)
*
***
****
G
%CRISPR efficiency
KO-Cas9
KO-Cas12a
H
% CRISPR efficiency
KI-Cas9
KI-Cas12a-nonTS
KI-Cas12a-TS

figure 3

A

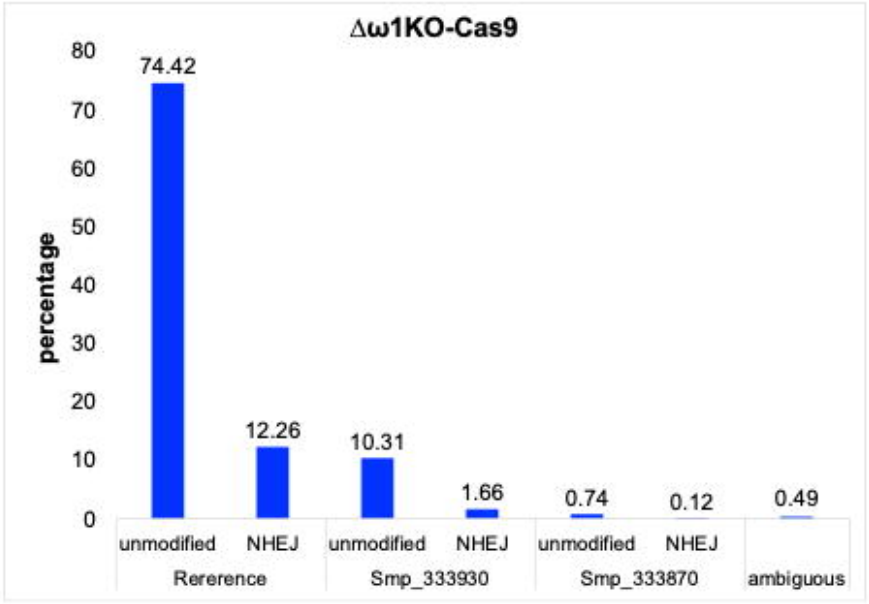

B

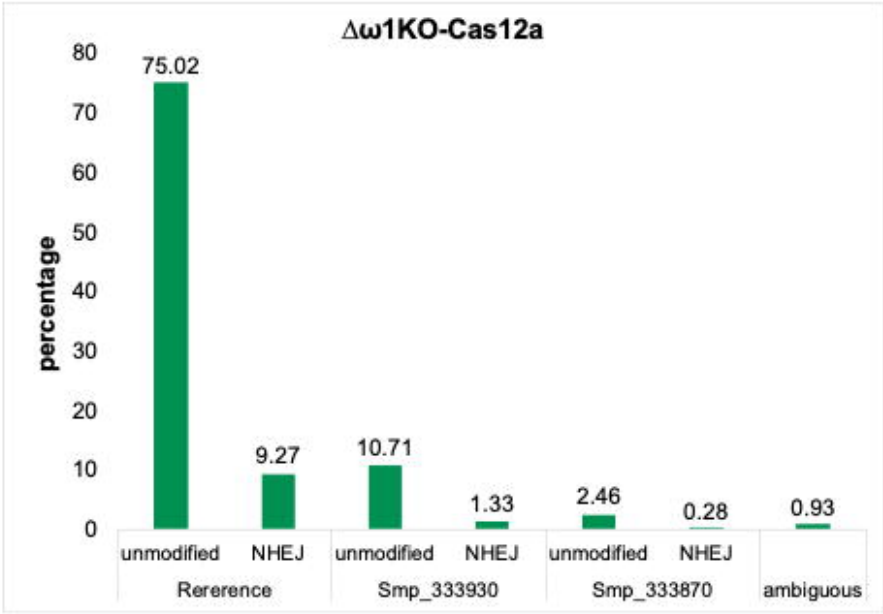

C

D

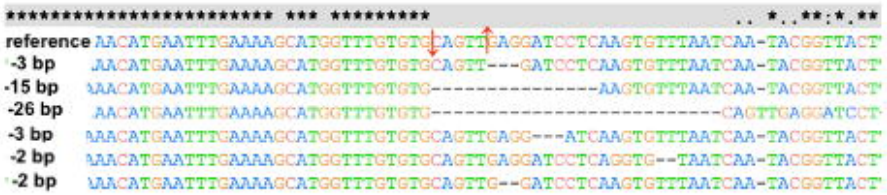

figure 4

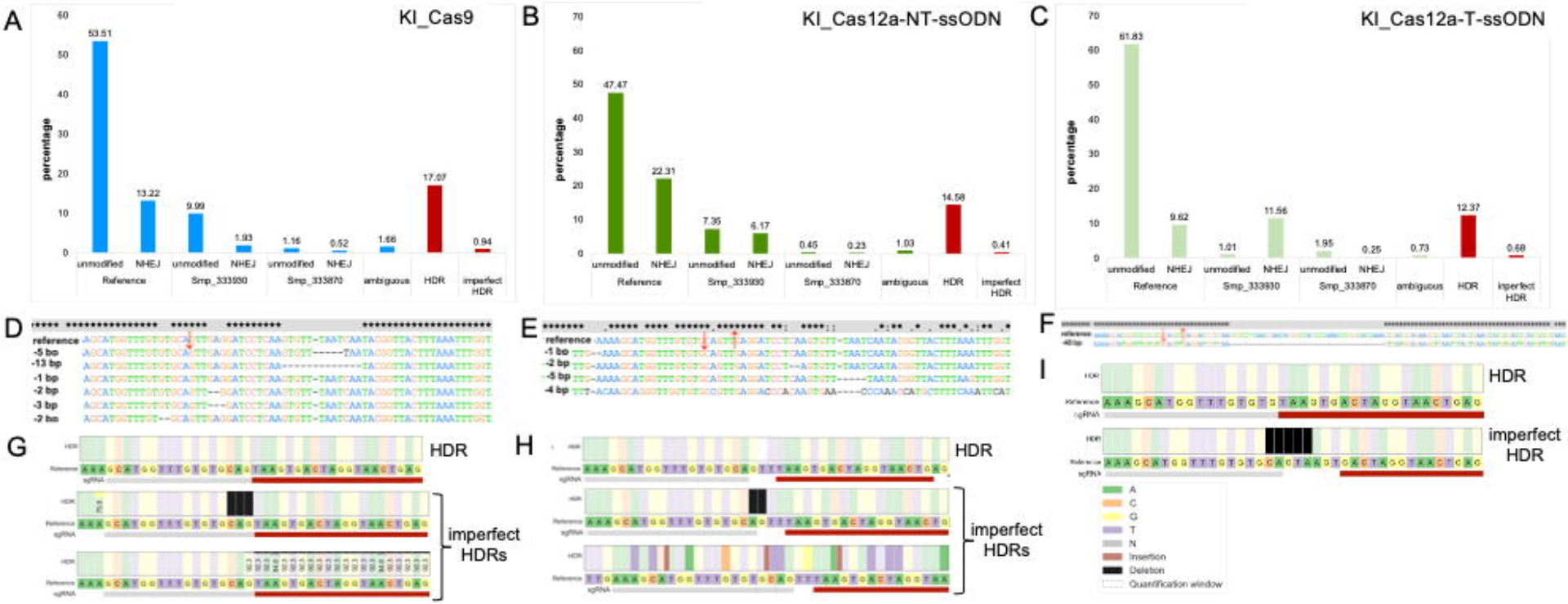
A
KI_Cas9
percentage
53.51
13.22
9.99
1.93
1.16
0.52
1.66
17.07
0.94
unmodified
NHEJ
Reference
Smp_333930
Smp_333870
ambiguous
HDR
imperfect HDR
B
KI_Cas12a-NT-ssODN
47.47
22.31
7.35
6.17
0.45
0.23
1.03
14.58
0.41
C
KI_Cas12a-T-ssODN
61.83
9.62
1.01
11.56
1.95
0.25
0.73
12.37
0.68
D
E
F
G
HDR
imperfect HDRs
H
HDR
imperfect HDRs
I
HDR
imperfect HDR
A
C
G
T
N
Insertion
Deletion
Quantification window

figure 5

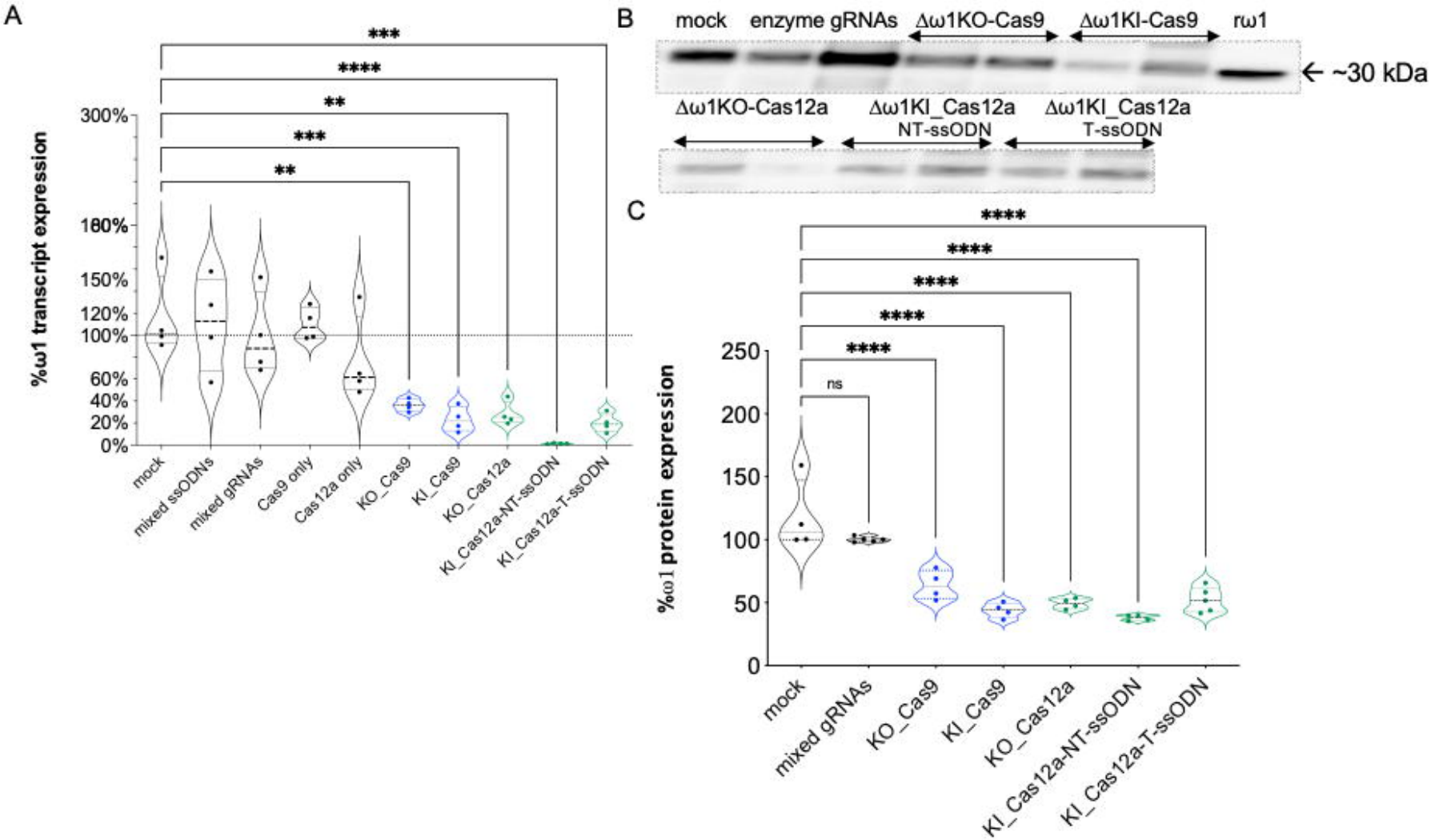
A
%ω1 transcript expression
300%
180%
150%
120%
100%
60%
40%
20%
0%
***
****
**
***
**
mock
mixed ssODNs
mixed gRNAs
Cas9 only
Cas12a only
KO_Cas9
KI_Cas9
KO_Cas12a
KI_Cas12a-NT-ssODN
KI_Cas12a-T-ssODN
B
mock
enzyme gRNAs
Δω1KO-Cas9
Δω1KI-Cas9
rω1
← ~30 kDa
Δω1KO-Cas12a
Δω1KI_Cas12a NT-ssODN
Δω1KI_Cas12a T-ssODN
C
%ω1 protein expression
250
200
150
100
50
0
****
****
****
****
****
ns
mock
mixed gRNAs
KO_Cas9
KI_Cas9
KO_Cas12a
KI_Cas12a-NT-ssODN
KI_Cas12a-T-ssODN